



Constraints on Chondrule Generation, Disk Dynamics, and Asteroid Accretion from the Compositions of Carbonaceous Meteorites

James F. J. Bryson¹ and Gregory A. Brennecke²

¹ Department of Earth Sciences, University of Oxford, South Parks Road, Oxford OX1 3AN, UK; james.bryson@earth.ox.ac.uk

² Lawrence Livermore National Laboratory, Livermore, CA, USA

Received 2021 January 9; revised 2021 February 21; accepted 2021 February 24; published 2021 May 17

Abstract

The elemental and isotopic compositions of meteorites are expected to reflect several key processes that occurred in the early solar system, including the migration of gas and dust throughout the protoplanetary disk, the formation of chondrules, and the accretion of the first planetary bodies. However, the specific origins of the various compositions measured among these rocks are currently poorly constrained, limiting our understanding of these processes. Here, we use previously measured elemental and isotopic compositions of chondrites and iron meteorites to identify that carbonaceous (CC) meteorites are mixtures of noncarbonaceous (NC) material, calcium–aluminum-rich inclusion (CAI) material, and CI (Ivuna-like) material, in varying proportions. These trends indicate that chondrules in CO (Ornans-like), CM (Mighei-like), CV (Vigarano-like), and TL (Tagish Lake) chondrites share near-identical average proportions of CI material, arguing that they were generated through the remelting of preexisting NC chondrules all in the same disk environment. Because this proportion likely evolved over space and time throughout the disk, this similarity argues that these chondrules originate from a restricted spatial region and time interval, favoring their generation through a localized event. Moreover, the compositions of CR (Renazzo-like) chondrites indicate that their constituents formed through mechanisms different from those in CO, CM, CV, and TL chondrites. The recovered proportions of CI material in CC iron meteorites and chondrites together also argue for evolution in either the predominant direction of dust and gas motion in the first ~ 10 au of the disk or the radial distance of planetesimal accretion throughout the CC reservoir.

Unified Astronomy Thesaurus concepts: Meteorites (1038); Meteorite composition (1037); Chondrules (229); Carbonaceous chondrites (200); Asteroids (72); Protoplanetary disks (1300); Iron meteorites (863); Planetesimals (1259); Isotopic abundances (867)

1. Introduction

Shortly after the ignition of the Sun, the solar system contained a colossal cloud of dust and gas known as the protoplanetary disk. Within just a few million years, trillions of submillimeter-scale solids formed from this disk and coalesced to create a spectrum of planetary bodies that included asteroids, comets, and ultimately the planets that we recognize today. The mechanisms by which these early solids formed and evolved in the disk as well as the processes by which they interacted with each other and the remaining gas and dust governed the chemical and physical properties adopted by these bodies. As such, these early processes played pivotal roles in establishing the long-term thermochemical evolutions of the different planetary bodies found throughout our solar system. Aggregates of these early solids, as well as fragments of the first planetary bodies that formed in the solar system, exist on Earth today in the form of meteorites. Through novel high-resolution and high-sensitivity techniques, these samples have recently provided several new insights into the evolution of the protoplanetary disk and the formation of the first solids. For instance, a number of measurements have revealed that the stable isotopic compositions of all meteorites fall into two distinct families (Warren 2011; Scott et al. 2018; Kruijer et al. 2019; Kleine et al. 2020; Bermingham et al. 2020). This dichotomy has been used to argue that these extraterrestrial rocks each originate from one of two reservoirs of material that existed in the protoplanetary disk that were spatially separated by a large feature (possibly Jupiter; Kruijer et al. 2017; Brasser & Mojzsis 2020; Lichtenberg et al. 2021) that hindered the

exchange of material between these regions. This restricted motion prevented disk-wide mixing and compositional homogenization, allowing the distinct composition of each reservoir to form and be retained over much of the disk’s lifetime. One key observation supporting this dichotomy is the $\epsilon^{94}\text{Mo}$ and $\epsilon^{95}\text{Mo}$ values (where ϵ denotes normalized isotopic concentration in parts per 10,000) of iron meteorites (fragments of the metallic cores of melted asteroids), rocky achondrites (fragments of the mantles and crusts of melted asteroids), and chondrites (fragments of unmelted asteroids), which together form two parallel lines when plotted against each other (Budde et al. 2016; Kruijer et al. 2017; Budde et al. 2019). Additionally, the isotopic compositions of a suite of other elements (including $\epsilon^{48}\text{Ca}$, $\epsilon^{50}\text{Ti}$, $\epsilon^{54}\text{Cr}$, $\epsilon^{62}\text{Ni}$, $\epsilon^{100}\text{Ru}$, and $\Delta^{17}\text{O}$ values, where Δ denotes the normalized non-mass-dependent isotopic concentration in parts per 1000) all form pairs of clusters when plotted against each other, further supporting the existence of separated reservoirs composed of material with isotopically distinct compositions in the protoplanetary disk (Warren 2011; Fischer-Godde & Kleine 2017; Bermingham et al. 2018; Schiller et al. 2018; Nanne et al. 2019; Worsham et al. 2019). In all of these cases, the same meteorite groups systematically share similar isotopic signatures and fall into the same families. As such, all meteorites can be primarily categorized as either noncarbonaceous (NC) or carbonaceous (CC) based on their isotopic compositions (named after the type of chondrite found within each family; Budde et al. 2016).

These isotopic signatures, as well as the elemental compositions of meteorites, are expected to reflect several key processes

that acted in the early solar system, including the addition, migration, and mixing of dust and gas from different regions of the protoplanetary disk, the formation of the first solid objects in the disk, and the accretion of the earliest planetary bodies. However, the origins of the different compositions measured among various meteorites are currently poorly constrained, critically limiting our understanding of the transformation of our solar system from a cloud of dust and gas to the chemically diverse collection of planetary bodies observed today. In this study, we explore these origins by examining previously measured compositions of CC chondrites and CC iron meteorites. Both of these types of meteorites are subcategorized into a number of groups that are each thought to originate from a distinct parent asteroid: CC chondrites into CI (Ivuna-like), CM (Mighei-like), CO (Ornans-like), CV (Vigarano-like), CK (Karoonda-like), CR (Renazzo-like), CB (Bencubbin-like), CH (high-metal-like), and TL (the ungrouped Tagish Lake chondrite); and CC iron meteorites into IIC, IID, IIF, IIIF, and IVB. Chondrites are lithified aggregates of the solids that existed in the protoplanetary disk, so CC chondrites provide a unique record of the material that existed throughout the CC reservoir. These meteorites consist of chondrules, refractory inclusions (calcium–aluminum-rich inclusions [CAIs] and amoeboid olivine aggregates [AOAs]), matrix, and metal grains in varying proportions (Scott & Krot 2014):

1. Chondrules are submillimeter- to millimeter-scale igneous spherules that ultimately originate from the melting and solidification of free-floating clumps of dust in the disk. They consist predominantly of silicate minerals, glassy mesostasis, metal, and sulfides, and typically make up $\sim 20\text{--}70$ vol% of CC chondrites depending on the group (Scott & Krot 2014). Many chondrules show evidence of multiple generations of melting captured by the persistence of relict grains, which formed in a previous chondrule generation and did not fully melt during the most recent remelting event.
2. CAIs are a minor component (<5 vol%; Scott & Krot 2014) of CC chondrites and are composed of various refractory minerals that formed through the direct condensation of hot nebula gas. The mineralogies and compositions of these objects have been used to argue that they formed close to the young Sun shortly after it ignited and subsequently migrated into the CC reservoir (Wood 2004). This formation history is consistent with the measured ages of CAIs, which identify them as the first solids to have formed in the solar system (Connelly et al. 2012).
3. The matrix is a mixture of a variety of fine-scale grains that were inherited from the protoplanetary disk and bind chondrules and refractory inclusions together. It makes up most of the remaining volume fraction of CC chondrites (typically $\sim 30\text{--}80$ vol% depending on the group, although can be as high as ~ 100 vol%; Scott & Krot 2014).

The present-day mineralogies of CC chondrites are diverse, ranging from consisting almost entirely of primary anhydrous minerals (Alexander et al. 2018a; Davidson et al. 2019a, 2019b) to being made up completely of secondary minerals that formed through reactions with water on their parent asteroids that was originally accreted as ice into their matrices (Howard et al. 2015; King et al. 2015, 2017). Together,

these properties demonstrate that the CC reservoir contained both material generated through high-temperature processes (melting and condensation) as well as a suite of primitive volatile-rich solids and water ice. CC iron meteorites and CC rocky achondrites are thought to originate from the cores and mantles, respectively, of asteroids that were originally composed of CC-chondrite-like material that experienced melting and differentiation. Hence, their elemental and isotopic compositions are also expected to reflect the make-up of the material that was present in the CC reservoir, although these signals can carry an overprint from differentiation. Given these formation histories, the elemental and isotopic compositions of both CC chondrites and CC iron meteorites are, therefore, expected to carry signatures of the various dynamic, thermal, and accretionary processes that acted in the protoplanetary disk.

A number of recent studies have proposed that the bulk elemental and isotopic compositions of CC chondrites originate from the mixture of chemically and isotopically distinct solids that existed in the early solar system. For instance, Burkhardt et al. (2019) and Gerber et al. (2017) identified that the isotopic and elemental compositions of refractory elements in both bulk CC chondrites and their chondrules can be expressed as mixtures of NC material (represented by ordinary and enstatite chondrites) and refractory objects (represented by CAIs). Moreover, Braukmuller et al. (2018) and Jacquet et al. (2016) proposed that most bulk CC chondrites contain a component that is similar in its relative elemental abundances to CI chondrites, a small group of meteorites (containing <10 members) that are essentially 100 vol% matrix and whose non-atmophile element compositions are unfractionated relative to the solar photosphere (Barrat et al. 2012). Together, these results indicate that CC meteorites could potentially be mixtures of “chondrule” material with refractory objects and CI-like material, an idea recently explored by Alexander (2019a); this model also contains a fourth component, which is water ice enriched in heavy oxygen isotopes. To date, these mixing models have either adopted an inverse approach that focuses on one type of element (e.g., refractory elements by Burkhardt et al. 2019; volatile elements by Braukmuller et al. 2018) or have been forward-models that allow both the proportions and the elemental and isotopic compositions of the end-members to vary, meaning that the calculated end-member compositions sometimes do not match those measured among different meteorite groups and components (Alexander 2019a).

In this study, we develop a new mixing model for the origins of the elemental and isotopic compositions of CC meteorites using a compilation of previously measured elemental and isotopic compositions from a suite of meteorites and their components. This model builds on previous studies by implementing an inverse approach that considers the compositions of NC and CC meteorites, chondrites and iron meteorites, and elements that cover a wide range of condensation temperatures. We use this model to explore the origins of the different components of CC chondrites, uncovering new constraints on the timings and locations of chondrule remelting that help to elucidate the generation of these enigmatic objects. Additionally, this model yields an origin for the NC–CC dichotomy that is rooted in the mixture of materials that originate from different regions of the protoplanetary disk, providing new constraints on the dynamics of gas, dust, and

early solids throughout the young solar system as well as the formation environments of the first planetary bodies.

2. Mixing Curves in CC Meteorites

Braukmuller et al. (2018) proposed that all elements fall into one of four categories based on their condensation temperature: refractory elements (50% condensation temperature, $T_{c,50} > 1400$ K), which exhibit approximately uniform enrichments in their Si-normalized concentrations in CC chondrites compared to CI chondrites by a factor of ~ 1 –1.4; main component elements ($1300 \text{ K} < T_{c,50} < 1400 \text{ K}$), which have approximately the same Si-normalized elemental abundances in CC chondrites as CI chondrites (differ by a factor of ~ 0.8 –1.1); slope-volatile elements ($800 \text{ K} < T_{c,50} < 1300 \text{ K}$), which exhibit monotonically decreasing Si-normalized concentrations with decreasing $T_{c,50}$ compared to CI chondrites; and plateau volatile elements ($T_{c,50} < 800 \text{ K}$), which display uniform depletions in Si-normalized concentrations compared to CI chondrites by a factor of ~ 0.1 –0.7 that are characteristic of each CC chondrite group. Given their uniform nature with $T_{c,50}$ and comparatively well-constrained isotopic and elemental compositions, we chose to focus on the concentrations of refractory, main component, and plateau volatile elements in this study. For the refractory and main component elements in CC chondrites, we examine the elemental and isotopic compositions of Ti and Cr, respectively, because these are lithophile elements whose isotopic compositions have been measured precisely for a large number of chondrites and their components (Trinquier et al. 2007, 2009; Qin et al. 2010; Olsen et al. 2016; Van Kooten et al. 2016; Gerber et al. 2017; Davis et al. 2018; Zhu et al. 2019; Schneider et al. 2020; Williams et al. 2020). For CC iron meteorites, we examine the isotopic compositions of Mo and Ni, respectively, because these are siderophile elements (so are therefore present in appreciable concentrations in iron meteorites, unlike Ti and Cr) whose compositions have also been relatively well studied in a number of iron meteorites as well as chondrites and their components (Burkhardt et al. 2011; Budde et al. 2016; Kruijer et al. 2017; Bermingham et al. 2018; Nanne et al. 2019; Budde et al. 2019; Worsham et al. 2019; Brennecka et al. 2020; Spitzer et al. 2020). For the plateau volatile elements, we examine the elemental compositions of six elements (Bi, Ag, Pb, Zn, Te, and Sn) that exhibit a number of desirable properties: their concentrations have been relatively well constrained in CC chondrites; they show a range of lithophile, siderophile, and chalcophile behaviors; their concentrations do not appear to be strongly dependent on redox state; they show minimal variability among NC chondrite groups. Our reasoning for not considering the isotopic compositions of these elements is discussed in Section 2.3. The adopted isotopic and chemical composition of each element used in this study in CC chondrites, CC iron meteorites, CAIs, CI chondrites, and NC chondrites are included in Table 1. Uncertainties on elemental concentrations have not been routinely reported throughout the literature, although these values are typically ± 5 wt% (e.g., Lodders 2003; Palme et al. 2014). CAIs can be categorized into six groups based on their compositions (Stracke et al. 2012). For the purposes of this study, we adopt the composition of type I CAIs as the representative value of refractory objects because they are seemingly the most abundant type and lack the characteristic elemental depletions of other CAI groups (e.g., Stracke et al. 2012; Brennecka et al. 2020). We also focus

largely on ordinary chondrites (OC) as representative NC meteorites rather than enstatite chondrites (EC) or Rumuruti chondrites (RC). This is because EC chondrites formed under more reducing conditions than OC and RC chondrites, which introduced a compositional signature for some elements to EC chondrites that is not present in OC, RC, or CC chondrites (presumably due to their formation in more oxidizing environments) so is not representative of large-scale mixing in the disk (Alexander 2019b). Additionally, the isotopic compositions of RC chondrites are sparsely measured compared to OC and EC chondrites. NC meteorites could have experienced a number of processes (e.g., mixing, chondrule formation, volatile loss, the addition of refractory materials, etc.) that gave these meteorites their specific chemical and isotopic signatures (Alexander 2019b). We do not explore these processes in this study and simply adopt the measured elemental and isotopic compositions of NC chondrites as potential end-members for the compositions of CC meteorites.

In the case where a series of meteorites formed through the mixture of varying proportions of different end-members, the chemical and isotopic compositions of these rocks will fall on the calculated mixing curve between these end-members. As such, we explored the potential origin of CC chondrites as mixtures of different materials in the protoplanetary disk by calculating mixing curves between NC, CAI, and CI material, and comparing the predicted trends to the measured compositions. If the measured compositions fall on any of the calculated mixing curves, we recovered the proportions of each end-member that recreate the composition of the meteorite. In the case where a composition is a mixture of more than two components, we first calculated a mixing curve between the nonrefractory components (i.e., the NC–CI mixing curve) and then calculated the mixing curve between each point along this first curve and CAIs (yielding nonrefractory–refractory mixing curves that represent mixtures of varying proportions of NC, CI, and CAI material). As such, we present two proportions: the NC–CI proportion (i.e., the proportions of the nonrefractory component recovered from the main component and plateau volatile elements) and the refractory–nonrefractory proportion (i.e., that recovered from the refractory elements, corresponding to the proportion of CAI material in a meteorite). The values of the proportions of CAI were recovered to the nearest 0.5 wt%, and the values of the proportions of CI and NC material were recovered to the nearest 1 wt%. Because we find that the concentrations of refractory elements and main component elements in a given meteorite are controlled separately by its amounts of CAI material and CI material, respectively (see Sections 2.1 and 2.2), our examination of the elemental and isotopic compositions of Cr in chondrites only yields the mass fraction of the NC versus CI material in a meteorite, and our examination of the elemental and isotopic compositions of Ti only yields the mass fraction of refractory versus nonrefractory material. As such, we report both of these mass fractions out of 100 wt% even though in reality the amounts of NC, CI, and CAI materials should together total 100 wt%. In the interest of consistency, we also report both of these proportions out of 100% when we recover them from the joint Ti and Cr isotopic compositions in chondrites and joint Mo and Ni isotopic compositions in iron meteorites, as well as reporting recalculated proportions of CI material that lead to the proportions of NC, CI, and CAI totaling 100 wt%.

Table 1
Adopted Elemental Concentrations (in ppm) and Isotopic Concentrations (in ϵ units) of the Meteorites and Meteorite Components in This Study

	Si	Ti	Mo	Cr	Ni	Bi	Ag	Pb	Zn	Te	Sn	$\epsilon^{50}\text{Ti}$	$\epsilon^{54}\text{Cr}$	$\Delta^{95}\text{Mo}$	$\epsilon^{62}\text{Ni}$
CC Chondrites															
CI	107000 ^{1,2}	440 ^{1,3}	0.961 ^{1,2}	2620 ^{1,2}	10600 ^{1,3}	0.112 ^{4,5,6,7}	0.204 ^{4,9,6,8}	2.59 ^{4,9,10}	312 ^{4,9,5,10,11,12}	2.28 ^{4,13}	1.54 ^{4,9,5}	1.85 ^{14,15,16}	1.56 ^{14,17,18,19}	22 ²²	0.2 ¹⁴
2 σ												0.12	0.06	34	0.14
CM	130000 ^{1,23,24,25}	619 ^{1,23,24,5,25}		3060 ^{1,23,24,25}		0.069 ^{4,23,6,7}	0.131 ^{4,9,23,7}	1.49 ^{4,9,24}	187 ^{4,9,24,11,12}	1.41 ^{4,13}	0.937 ^{4,9}	3.01 ^{14,15,20,16}	1.02 ^{14,17,18,21,19}		
2 σ												0.1	0.08		
CO	160000 ^{1,23,26}	765 ^{1,25}		3550 ^{1,23}		0.035 ^{4,23,7}	0.08 ^{4,9,23}	0.839 ^{4,9,23}	100 ^{4,9,23,11,12,27}	0.863 ^{4,9}	0.559 ^{4,9,23}	3.77 ^{14,15,16}	0.77 ^{14,17,18,19}		
2 σ												0.5	0.33		
CV	160000 ^{1,28,29}	899 ^{1,28,29}		3600 ^{1,28,29}		0.051 ^{4,23,6,7}	0.097 ^{4,9,6,8}	1.07 ^{4,9}	111 ^{4,9,30,12}	0.896 ^{4,13}	0.688 ^{4,9}	3.49 ^{14,15,20,16}	0.87 ^{14,17,18,19}		
2 σ												0.2	0.07		
CK	159000 ^{1,25}	940 ^{1,31}		3610 ^{1,30}		0.02 ^{1,32}	0.055 ⁹	0.75 ⁹	97 ¹	0.8 ¹	0.49 ¹	3.63 ^{14,15,16}	0.48 ^{14,17,18}		
2 σ												0.4	0.3		
CR	158000 ^{1,33}	656 ¹		3790 ^{1,34}			0.04 ^{4,9}	0.467 ^{4,9}	60.1 ^{4,9,35}	0.496 ^{4,13}	0.301 ^{4,9}	2.74 ^{14,15}	1.31 ^{14,17,18}		
2 σ												1.17	0.1		
TL	116000 ^{1,36,37}	514 ^{1,5,36,37}		2710 ^{1,36,37}		0.088 ^{4,5,38}	0.148 ^{4,9,5,37,38}	1.73 ^{4,36,37}	210 ^{4,9,5,11,36,37,38}	1.64 ⁴	1.02 ^{4,9,5,36,37,38}	2.76 ¹⁵	1.19 ³⁹		
2 σ												0.26	0.15		
Group 1 CAIs	131460 ²⁸	7884 ²⁸	7 ⁴⁰	624 ²⁸	900 ¹⁴							9 ¹⁴	7 ¹⁴	124 ⁴¹	0.55 ⁴²
2 σ												0.53	1	14	0.24
NC Chondrites															
H	169000 ^{43,23}	600 ^{43,23}	1.505 ^{43,23}	3660 ^{43,23}	16000 ^{43,23}	0.017 ^{43,23}	0.054 ⁸	0.798 ⁸	48 ²⁷	0.32 ⁴⁴	0.43 ²⁷	-0.64 ^{14,15,16,20}	-0.36 ^{14,17,18}	-15 ⁴¹	-0.06 ^{14,45,46}
2 σ												0.17	0.08	8	0.03
L	185000 ^{43,23}	630 ^{43,23}	1.060 ^{43,23}	3880 ^{43,23}	12000 ^{43,23}	0.014 ^{43,23}	0.029 ⁸	0.652 ⁸	51 ²⁷	0.22 ⁴⁴	0.39 ²⁷	-0.63 ^{14,15,16}	-0.4 ^{14,17,18}	-15 ⁴¹	-0.04 ^{14,45,46}
2 σ												0.08	0.1	8	0.03
LL	189000 ^{43,23}	620 ^{43,23}	0.880 ^{43,23}	3740 ^{43,23}	10200 ^{43,23}	0.016 ^{43,23}	0.05 ⁸	0.494 ⁸	65.5 ²⁷	0.35 ⁴⁴	0.37 ²⁷	-0.67 ^{14,15,16}	-0.42 ^{14,17}	-15 ⁴¹	-0.07 ^{14,45,46}
2 σ												0.08	0.07	8	0.03
R	178000 ^{43,47}	570 ^{43,47}		3570 ^{43,48}									0.16 ^{14,17}		
2 σ													0.5		
EH	167000 ^{43,23}	450 ^{43,23}		3150 ^{43,23}								-0.14 ^{14,15,16}	0.04 ^{14,14,17}	-10 ⁴¹	0.03 ^{14,45,46}
2 σ												0.07	0.08	9	0.03
EL	186000 ^{43,23}	550 ^{43,32}		3180 ^{43,49}								-0.28 ^{14,16}	0.04 ^{14,14,17}	-7 ⁴¹	-0.03 ^{14,45,46}
2 σ												0.17	0.07	9	0.07
CC Iron Meteorites															
IIC														22 ⁴¹	0.16 ^{14,50}
2 σ														8	0.08
IID														31 ⁴¹	0.19 ^{14,50}
2 σ														5	0.08
IIIF														28 ⁴¹	0.09 ^{14,50}
2 σ														11	0.04
IIIF														27 ⁴¹	0.12 ^{14,50}
2 σ														8	0.08
IVB														24 ⁴¹	0.08 ^{14,50}
2 σ														8	0.04

Note. TL: Tagish Lake ungrouped chondrite. The explicit values of the elemental concentrations in CC chondrites are taken from Alexander (2019b), Hellmann et al. (2020), and Braukmuller et al. (2018). The explicit values of the elemental concentrations in NC chondrites are included as references. The explicit values and uncertainties of all isotopic concentrations were taken from Burkhardt et al. (2019), Spitzer et al. (2020), Kleine et al. (2020), Render et al. (2018), Petit et al. (2011), and Trinquier et al. (2009). The predominant original sources of the measured elemental and isotopic concentrations are included as references.

References. 1. Alexander (2019a), 2. Palme et al. (2014), 3. Lodders (2003), 4. Hellmann et al. (2020), 5. Friedrich et al. (2002), 6. Wang et al. (2015), 7. Laul et al. (1970), 8. Schönbächler et al. (2008), 9. Braukmuller et al. (2018), 10. Barrat et al. (2012), 11. Luck et al. (2005), 12. Pringle et al. (2017), 13. Braukmuller et al. (2019), 14. Burkhardt et al. (2019), 15. Trinquier et al. (2009), 16. Zhang et al. (2012), 17. Trinquier et al. (2007), 18. Qin et al. (2010), 19. Shukolyukov & Lugmair (2006), 20. Zhang et al. (2011), 21. Göpel et al. (2015), 22. Kleine et al. (2020), 23. Wasson & Kallemeyn (1988), 24. Hewins et al. (2014), 25. Wolf & Palme (2001), 26. Jarosewich (1990), 27. Creech & Moynier (2019), 28. Stracke et al. (2012), 29. Jarosewich et al. (1987), 30. Wasson et al. (2013), 31. Kallemeyn et al. (1991), 32. Lodders & Fegley (1998), 33. Mason & Wiik (1962), 34. Kallemeyn et al. (1994), 35. Bischoff et al. (1993), 36. Brown et al. (2000), 37. Blinova et al. (2014a), 38. Wolf et al. (2005), 39. Petit et al. (2011), 40. Burkhardt et al. (2011), 41. Spitzer et al. (2020), 42. Render et al. (2018), 43. Alexander (2019b), 44. Fehr et al. (2018), 45. Steele et al. (2012), 46. Tang & Dauphas (2014), 47. Bischoff et al. (2011), 48. Kallemeyn et al. (1996), 49. Kong et al. (1997), 50. Nanne et al. (2019).

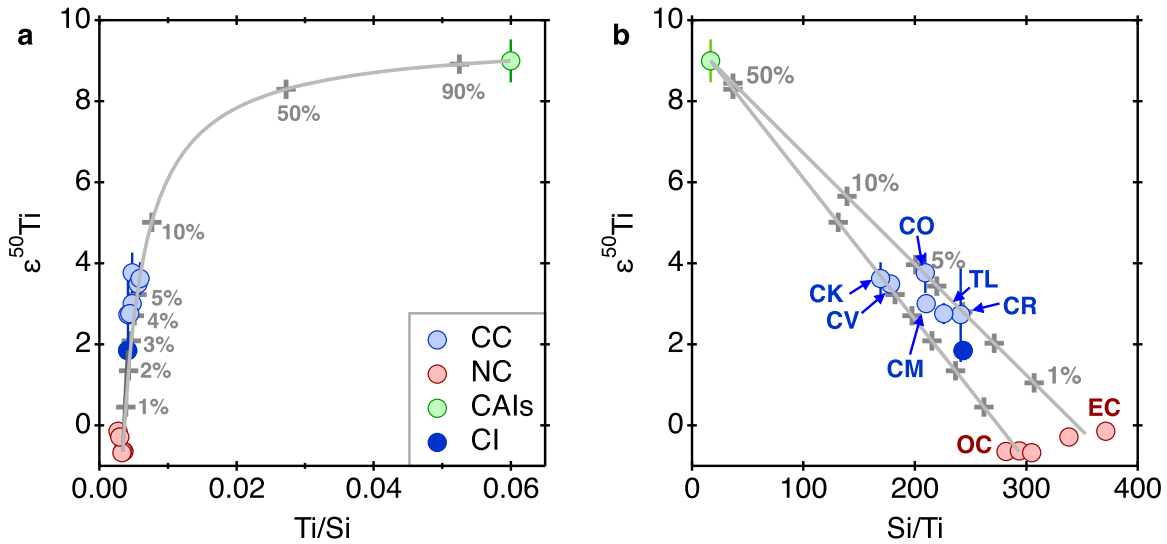


Figure 1. $\epsilon^{50}\text{Ti}$ values for CC chondrites, NC chondrites, and group 1 CAIs as a function of (a) Ti/Si and (b) Si/Ti. The calculated mixing curves from NC material (OC chondrites in a, and OC chondrites and EC chondrites separately in b) to group 1 CAIs are shown by the light gray lines. CC chondrites fall on or very close to these curves, indicating that the bulk elemental and isotopic compositions of these meteorites originates from the mixture of NC material with a small amount ($\lesssim 6$ wt%) CAI material. TL: Tagish Lake ungrouped chondrite.

The elemental composition of a mixture of end-members, C_{mix} , is calculated as

$$C_{\text{mix}} = \sum C_i P_i, \quad (1)$$

where C_i is the mass of the element of interest in component i , and P_i is the mass fraction of that component. We consider the elemental compositions of a meteorite or meteorite component normalized to its Si concentration to negate the effects of dilution by metal or water and to account for different analytical totals. The isotopic composition of a given element in a mixture, I_{mix} (in ϵ units), is calculated as

$$I_{\text{mix}} = \frac{\sum C_i I_i P_i}{\sum C_i P_i}, \quad (2)$$

where I_i is the isotopic composition (ϵ value) of component i . The ϵ values are calculated using

$$\epsilon^j X = \left(\left(\frac{\frac{jX}{kX}_{\text{samp}}}{\frac{jX}{kX}_{\text{stand}}} \right) - 1 \right) \times 10000, \quad (3)$$

where $^j X$ and $^k X$ are the abundances of two isotopes of element X , respectively, and the subscripts “smp” and “stand” denote the sample and recognized terrestrial standard, respectively. We also use Δ notation for ^{95}Mo , which removes the effect of s -process variations on the composition of ^{95}Mo and isolates just the effect of variable r -process material on the composition of this isotope (Kleine et al. 2020) and is defined as

$$\Delta^{95}\text{Mo} = (\epsilon^{95}\text{Mo} - 0.596 \times \epsilon^{94}\text{Mo}) \times 100. \quad (4)$$

Finally, the uncertainties that we report on the recovered proportions of CI and CAI material in CC iron meteorites, bulk CC chondrites, CC chondrules, and CC matrix were calculated directly from the measured 2σ uncertainties on their values of $\epsilon^{54}\text{Cr}$, $\epsilon^{50}\text{Ti}$, $\epsilon^{62}\text{Ni}$, and $\Delta^{95}\text{Mo}$ using Equation (2). Because the main source of uncertainty among the data that we considered is that on the measured isotopic compositions, we treat the uncertainties on the proportions of CI and CAI

material as the same when we recover these from the joint elemental and isotopic composition of Cr or Ti individually as well as the joint Cr and Ti isotopic compositions of CC chondrites. Our reported uncertainties on the proportion of CI material recovered from the elemental concentrations of plateau volatile elements correspond to the 2σ value of the distribution of the proportions calculated from the six separate plateau volatile elements that we considered. The uncertainties in the calculated matrix mass fractions correspond to the typical variation observed in the matrix volume fraction among different samples, which is approximately ± 10 vol% (e.g., Schrader et al. 2011; Gattacceca et al. 2020). The uncertainties on the accretion ages of CC iron meteorite and CC chondrite parent bodies are taken from Kleine et al. (2020); the effect of the comparatively large uncertainties on the measured Hf-W ages of CC iron meteorites is discussed further in Section 3.4.

2.1. Refractory Elements

Burkhardt et al. (2019) identified that the isotopic and elemental compositions of a number of refractory elements in bulk CC chondrites (including CI chondrites) fall on mixing curves that extend from bulk NC material to CAI material, indicating that the refractory element concentrations of CC chondrites originate in part from the mixture of NC and CAI material (demonstrated here using Ti; Figure 1). CAI material could be present in a number of forms in these meteorites, including as bulk CAIs themselves, as the dust from which CAIs formed (as a component of the matrix, although this dust likely exhibits a Ti/Si value similar to CI chondrites so would correspond to a different mixing line; Schneider et al. 2020), and as a component within chondrules (Gerber et al. 2017). The proportion of CAI material, P_{CAI} , ranges from ~ 2.5 wt% in CI chondrites to ~ 6 wt% in CK chondrites (Table 2). These values of P_{CAI} are typically about twice the volume fraction of bulk CAIs observed petrographically in each CC chondrite group (Scott & Krot 2014), supporting the existence of some CAI material as a component within chondrules and as small CAIs that are difficult to discern from petrographic observations. Burkhardt et al. (2019) recovered very similar proportions of

Table 2
Recovered Values of P_{CAI} , $P_{\text{Cl,Cr}}$, $P_{\text{Cl,Ni}}$, and $P_{\text{Cl,vtl}}$, and Associated 2σ Uncertainties, Calculated Using Equation (2)

		P_{CAI} (wt%, Figure 1)	P_{CAI} (wt%, Figures 2(c), (d))	2σ on P_{CAI} (wt%)	$P_{\text{Cl,Cr}}$ (wt%, Figures 2(a), (b))	$P_{\text{Cl,Cr}}$ or $P_{\text{Cl,Ni}}$ (wt%, Figures 2(c), (d))	2σ on $P_{\text{Cl,Cr}}$ or $P_{\text{Cl,Ni}}$ (wt%)	Adjusted Proportion of CI Material (wt%) ^a	$P_{\text{Cl,vtl}}$ (wt%, Figure 3)	2σ on $P_{\text{Cl,vtl}}$ (wt%)
CC chondrites	CI	2.5	2.5	0.2	100	100	2	98	100	0
	CM	4	4.5	0.2	80	78	3	75	57	7
	CO	4.5	6	1.3	66	65	14	61	20	11
	CV	5.5	5.5	0.5	71	70	3	66	28	10
	CK	6	6.5	1.0	55	50	15	47	14	15
	CR	3	3.5	2.5	91	90	4	87	2	14
	TL	3.5	4	0.5	85	85	6	82	72	10
IIsCC iron meteorites	IIC		3.5	1.7		87	26	84		
	IID		4	1.2		97	25	93		
	IIF		5.5	2.6		61	14	58		
	IIIF		5	1.8		73	27	69		
	IVB		5.5	1.7		54	15	51		

Notes. The figure from which each of these values are recovered is included in the column title. The values of P_{CAI} in all CC chondrites and CC iron meteorites can be decreased by up to 2.5 wt% depending on the amount of CAI material in CI chondrites. TL: Tagish Lake ungrouped chondrite.

^a Proportion of CI material adjusted so that the proportions of NC, CI, and CAI material calculated from Figures 2(c) and (d) total 100 wt%.

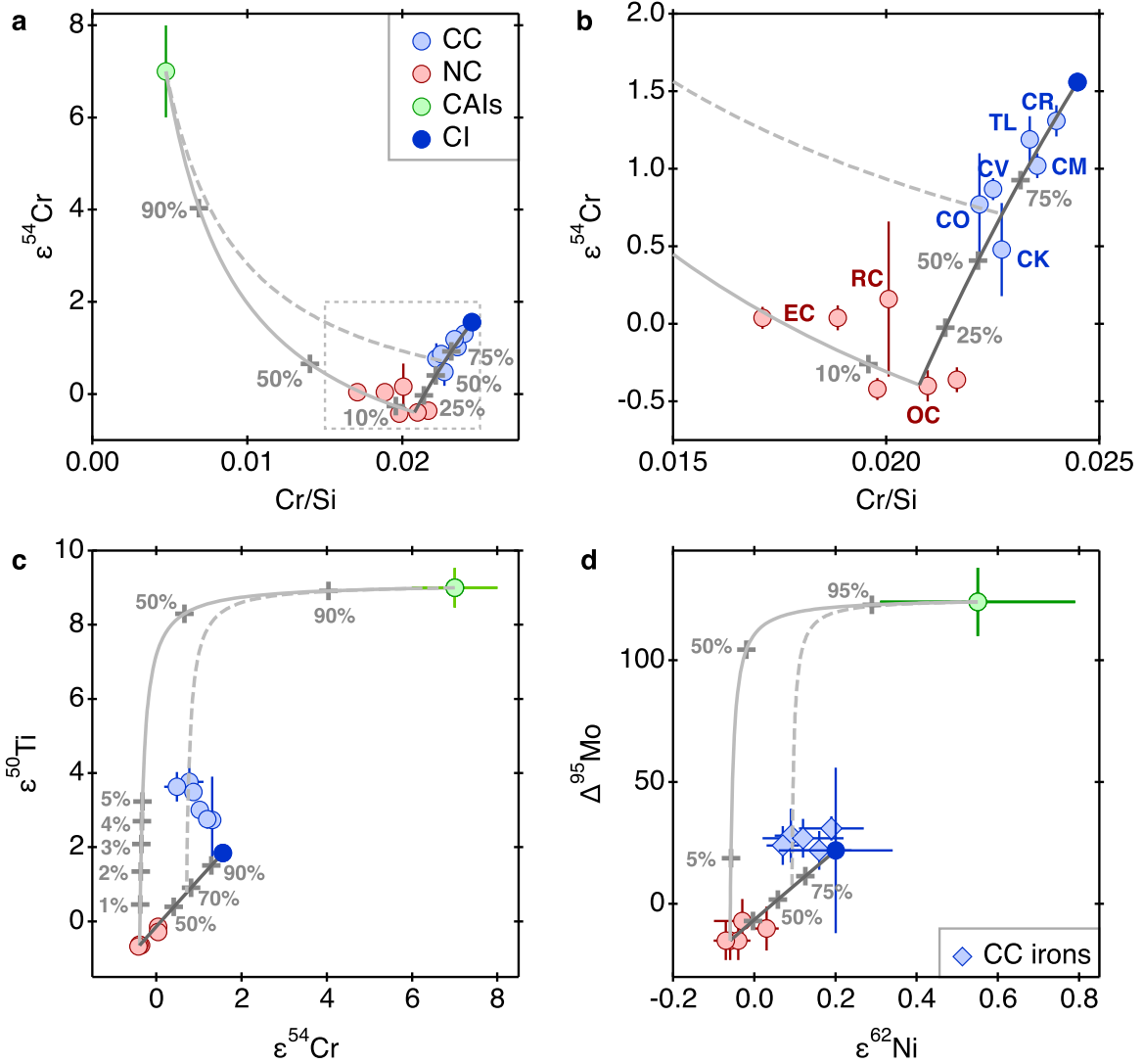


Figure 2. (a) $\varepsilon^{54}\text{Cr}$ values for CC chondrites, NC chondrites (OC, EC, and RC), and group 1 CAIs as a function of Cr/Si. (b) Zoom in of the dotted box in (a) to highlight the nonrefractory mixing curve. (c) $\varepsilon^{50}\text{Ti}$ and $\varepsilon^{54}\text{Cr}$ values for CC chondrites, NC chondrites (OC and EC; the values are similar enough that different OC and EC are groups overlap and are difficult to distinguish), and group 1 CAIs. (d) $\Delta^{95}\text{Mo}$ and $\varepsilon^{62}\text{Ni}$ values for CC iron meteorites, NC chondrites, and group 1 CAIs. In all of these plots, the NC–CAI mixing curve is shown by the solid light gray line and the NC–CI mixing curve is shown by the solid dark gray line. The mixtures of NC, CI, and CAI components that recreate CO chondrites in (a), (b), and (c) and the IIF iron meteorites in (d) are shown by the dashed light gray line (calculated by first mixing between NC and CI components, and then mixing from a given proportion along this nonrefractory line to CAIs). The proportion of the CI component in CC chondrites and iron meteorites was calculated from the intersection of the dashed light gray line with the solid dark gray line. The error bars are smaller than the points in some cases. TL: Tagish Lake ungrouped chondrite.

CAI material ($\sim 3\text{--}7\text{ wt\%}$) from the analysis of a number of refractory elements that display a wide range of $T_{c,50}$ values, indicating that the elemental and isotopic compositions of several refractory elements in bulk CC chondrites originate in part from the mixing of NC and CAI material.

2.2. Main Component Elements

The elemental and isotopic compositions of Cr in CC chondrites also fall on a mixing curve (Figures 2(a), (b)). However, this curve extends from average bulk OC material to CI chondrites, rather than to CAI material. This result demonstrates that CI chondrites cannot be expressed solely as a mixture of NC and CAI material (as suggested by refractory element concentrations), and argues that a distinct reservoir of material with an isotopic composition similar to that of CI chondrites existed in the protoplanetary disk. This result also demonstrates that the remaining CC chondrite groups contain a

component that originates from this reservoir, similar to an idea proposed by Schiller et al. (2018). This component could have been introduced to CC chondrites either through the initial mixing of populations of dust with NC and CI isotopic compositions from which chondrules subsequently formed to generate the chondrites themselves, or through the mixing of CI dust with bulk preaccretionary NC chondrite material (i.e., a mixture of NC chondrules and NC dust).

Due to the low concentration of Cr in CAIs ($\text{Cr/Si} = 0.0047$) compared to bulk chondrites (e.g., $\text{Cr/Si} = 0.022$ in CO chondrites; Figures 2(a), (b); Table 1), the proportion of CAI material identified from the refractory element compositions ($\lesssim 6\text{ wt\%}$) will have introduced small changes to the $\varepsilon^{54}\text{Cr}$ and Cr/Si values that are largely within the uncertainties of the measured isotopic compositions (Figure 2(b)). For instance, 10 wt% CAI is expected to have only changed the Cr/Si value by 0.0012 and the $\varepsilon^{54}\text{Cr}$ value by 0.13. As such, the measured

Cr isotopic and elemental concentrations are consistent with the small proportions of CAI material derived from the refractory element concentrations ($\lesssim 6$ wt%), although reliable proportions of CAI material in CC chondrites cannot be determined using Cr concentrations. Instead, the Cr concentrations of CC chondrites predominantly reflect the proportions of nonrefractory material (i.e., NC versus CI material), with the proportion of CI-like material in this nonrefractory component, $P_{\text{CI,Cr}}$, ranging from ~ 55 wt% in CK chondrites to ~ 91 wt% in CR chondrites (Table 2). Combined with the refractory element concentrations, these observations are consistent with the main component element concentrations of CC chondrites being a mixture of NC material, CI material, and CAI material, in varying proportions.

The joint $\epsilon^{50}\text{Ti}$ and $\epsilon^{54}\text{Cr}$ compositions of a number of chondrites and rocky achondrites (Figure 2(c)) have been one of the key observations supporting a dichotomy among NC and CC meteorites (Warren 2011). However, the origin of this dichotomy, as well as the origin of the variations within the NC and CC families, have remained largely elusive. The $\epsilon^{50}\text{Ti}$ and $\epsilon^{54}\text{Cr}$ values of CC chondrites each fall on separate nonrefractory–refractory mixing curves (Figure 2(c)), supporting our proposal that CC chondrites are mixtures of NC, CAI, and CI material. Moreover, the variations in the isotopic compositions among CC chondrites can be explained by variations in the proportions of these three components. The proportions of these components recovered from the combined $\epsilon^{50}\text{Ti}$ and $\epsilon^{54}\text{Cr}$ values (P_{CAI} ranging from ~ 2.5 to 6.5 wt%; $P_{\text{CI,Cr}}$ ranging from 50 – 90 wt%; Table 2) are almost identical to those recovered from the elemental and isotopic concentrations of Ti (P_{CAI} ranging from ~ 2.5 to 6 wt%; Figure 1) and Cr ($P_{\text{CI,Cr}}$ ranging from ~ 55 to 91 wt%; Figures 2(a), (b)) individually. As such, the isotopic dichotomy between NC and CC meteorites can be explained by the mixing of CAI, CI, and NC material in varying proportions, an idea similar to that proposed by Trinquier et al. (2009).

Five of the recognized iron meteorite groups have isotopic compositions that classify them as CC meteorites (IIC, IID, IIF, IIIF, and IVB groups). Following the trends identified from the Ti and Cr concentrations, it is possible that the material that makes up these iron meteorite groups could have formed through the melting and differentiation of mixtures of NC, CAI, and CI material. To explore whether this is the case, we examined the isotopic compositions of siderophile elements in CC iron meteorites. The isotopic compositions of Mo (siderophile refractory element) and Ni (siderophile main component element) in CC iron meteorites display similar patterns to those of the lithophile elements in CC chondrites, with the isotopic compositions of each of the iron meteorites also falling on separate nonrefractory–refractory mixing curves (Figure 2(d)). This observation indicates that the compositions of CC iron meteorites can also be expressed as mixtures of NC, CAI, and CI material. Moreover, the proportions of CI ($P_{\text{CI,Ni}}$), NC, and CAI materials recovered from CC iron meteorites (P_{CAI} ranging from ~ 3.5 to 5.5 wt%; $P_{\text{CI,Ni}}$ ranging from ~ 61 to 97 wt%; Table 2) isotopic compositions occupy very similar ranges to those recovered from CC chondrites (P_{CAI} ranging from ~ 2.5 to 6.5 wt%; $P_{\text{CI,Cr}}$ ranging from ~ 50 to 90 wt%; Table 2). As such, the compositions of all CC meteorites can be expressed as mixtures of NC, CI, and CAI material, in varying proportions.

2.3. Plateau Volatile Elements

The mass-dependent isotopic compositions of a number of plateau volatile elements in CC chondrites (e.g., Zn, Rb, Te) vary with their Si-normalized elemental concentration, and CI chondrites regularly display extreme values in both the isotopic concentration and Si-normalized elemental concentrations of these elements (Pringle & Moynier 2017; Pringle et al. 2017; Fehr et al. 2018; Hellmann et al. 2020). These properties are consistent with the elemental and isotopic compositions of plateau volatile elements in CC chondrites being mixtures of a volatile-poor material and CI material. However, the isotopic compositions of plateau volatile elements in NC chondrites typically occupy large ranges of values (e.g., -1.08 to 0.58 for $\delta^{122/118}\text{Sn}$ among different NC chondrites compared to 0.279 to 0.752 for CC chondrites; Creech & Moynier 2019), possibly due to parent body metamorphism (Schönbächler et al. 2008; Pringle & Moynier 2017; Pringle et al. 2017; Fehr et al. 2018; Creech & Moynier 2019). Because there is such a wide range of possible mixing curves that can be drawn from the breadth of NC isotopic compositions, it is difficult to demonstrate with certainty that the isotopic compositions of plateau volatile elements in CC chondrites fall on the mixing curve between pristine NC chondrites and CI chondrites (like they do for refractory and main component elements), although this is certainly consistent with the range of measured isotopic compositions of NC chondrites.

On the other hand, the elemental compositions of plateau volatile elements in NC chondrites often display far less variability. Following Braukmuller et al. (2018), we treat the compositions of these elements within CC and OC chondrites as flat at a value that is characteristic of each group (Figure 3(a)), with any deviation from this flat shape being due to uncertainties in the measurements and natural variations among samples. The various components within chondrites exhibit widely different plateau volatile element concentrations, with chondrules being volatile-depleted (containing ~ 13 wt% the volatile element concentration of CI chondrites) and unprocessed dust grains in the matrix containing CI-like elemental ratios (Hellmann et al. 2020). This low plateau volatile element concentration of chondrules compared to matrix is presumably a result of the high-temperature formation of chondrules (during which these elements could have been readily lost from a chondrule) and comparatively pristine nature of matrix. As such, similar to their Cr isotopic composition, the plateau volatile element concentrations of these meteorites could have been introduced either by forming chondrules from a population of dust that exhibited CI elemental ratios (which could have been a mixture of CI dust and NC dust, both of which likely displayed such elemental ratios) or the addition of CI dust to bulk NC chondrite material (NC chondrules and NC dust). In the latter case, the proportions of CI material in CC chondrites (i.e., the excess in volatile element concentration over NC chondrites), $P_{\text{CI,vil}}$, are shown in Figure 3(b) and are included in Table 2. These values vary from essentially 0 wt% in CR chondrites (i.e., these meteorites do not show a significant excess in plateau volatile elements compared to OC meteorites) to 72 wt% in the Tagish Lake ungrouped chondrite. These values are broadly similar to those recovered by Braukmuller et al. (2018; which range from ~ 15 to 70 wt%), with any differences arising from our choice of volatile-poor end-member (NC chondrites versus volatile-free material) and our use of Equation (1) applied to both the Si and

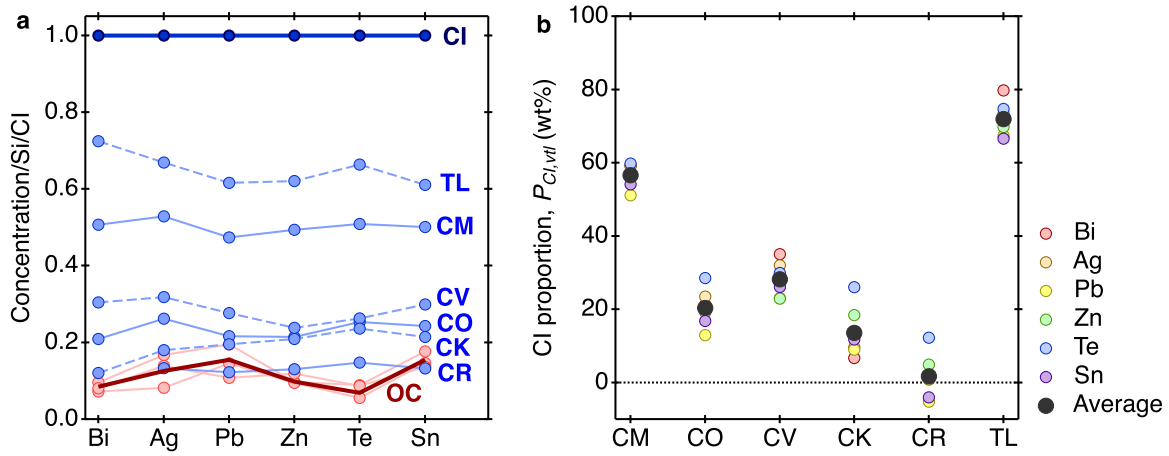


Figure 3. (a) The Si- and CI-normalized concentrations of six plateau volatile elements in CC and OC chondrites. The three separate OC chondrite groups (H, L, and LL) are shown by the pink points and lines, and the average OC value is shown by the bold dark red line. (b) The proportion of CI chondrite material within each CC chondrite group calculated from the mixing curves of OC chondrites with CI chondrites for each of the six plateau volatile elements. The scatter in the proportions calculated from each of the six plateau volatile elements results from the variability in both OC and CC chondrite compositions. TL: Tagish Lake ungrouped chondrite.

plateau volatile element concentrations to recover these proportions rather than assuming a single linear variation between the end-members.

3. The Proportions of NC, CAI, and CI Material in CC Meteorites

3.1. Mixtures in CC Meteorites

The elemental and isotopic compositions of the CC meteorites examined in this study can be expressed as mixtures of three components with varying proportions: CAI, CI, and NC material. As suggested by Alexander (2019a), there was also likely a fourth component that contributed to the overall elemental and isotopic compositions of these meteorites, which was water enriched in heavy oxygen isotopes. This final component is not evident in our study because we have not considered the compositions of O or H.

The recovered proportions of CAI material (from the refractory–nonrefractory mixing curves) and NC and CI material (from NC–CI mixing curves) within CC meteorites are shown in Figure 4. In the case of CC chondrites, the proportion of CAI material and CI material can be recovered from the elemental and isotopic composition of Ti and Cr individually (Figures 1 and 2(a) and (b)) as well as the joint Ti and Cr isotopic compositions of a chondrite (Figure 2(c)). As such, we present two values for P_{CAI} and $P_{CI,Cr}$ for CC chondrites in Table 2, which are very similar for each meteorite group. In the interest of clarity, we only present the P_{CAI} and $P_{CI,Cr}$ values recovered from Figure 2(c) in Figure 4.

In both iron meteorites and chondrites, the amounts of NC and CAI material covary (i.e., as one increases, the other increases), while both of these proportions vary in the opposite sense to the amount of CI material. As such, the mixture of materials in the protoplanetary disk appears to have been between CI material and a second component that was itself a mixture of NC and CAI material. This relationship argues that NC and CAI material were present together either at one time or in one location in the disk, while CI material was present at a second time or second location in the disk, and that these two families of materials mixed together in varying proportions across space and/or time to generate bulk CC chondrites. Because the accretion ages of CC (~1–4 Myr after CAI

formation) and NC (~0–2.5 Myr after CAI formation) parent bodies overlap when considering both iron meteorite and chondrite parent bodies (Sugiura & Fujiya 2014; Doyle et al. 2015; Kruijer et al. 2017; Kleine et al. 2020), NC and CAI material likely originated from one spatial region of the disk while CI material likely originated from a second region. NC chondrites contain comparatively low amounts of water (~0.12 wt% H in OC chondrites; Alexander et al. 2018b) and CAIs are thought to originate from close to the young Sun (Wood 2004), suggesting that NC and CAI material are associated with the inner disk. Conversely, CI chondrites are rich in water (~0.8–1 wt% H; Piani et al. 2020) and contain low CAI abundances (Table 2; Figure 4), suggesting that CI material is associated with the outer to distal regions of the disk.

3.2. The Proportions of CAI Material in CC Meteorites

As demonstrated by Burkhardt et al. (2019) and shown in Figure 1, the elemental and isotopic compositions of refractory elements in all CC chondrites, including CI chondrites, can be expressed as a mixture of NC and CAI material. However, as shown in Figure 2 and discussed in Section 2.3, this is not the case for Cr isotopic and elemental concentrations, where CI chondrites are an end-member in a mixing model with NC material. As such, CI chondrites should also be an end-member in the Ti isotopic and elemental compositions. The values of $\epsilon^{50}\text{Ti}$ and Ti/Si for CI chondrites fall on the NC–CAI mixing curve (Figure 1), which has two possible explanations. First, CI chondrites could be free of CAI material and their compositions happen to fall on this mixing curve. This scenario is consistent with the general absence of bulk CAIs in petrographic observations of CI chondrites (Scott & Krot 2014). In this case, mixing between NC and CI material will move the composition of the nonrefractory component of CC chondrites along the same mixing line as mixing with CAI material. As such, the $\epsilon^{50}\text{Ti}$ and Ti/Si values of the bulk CC chondrites can still be expressed as a mixture of NC, CAI, and CI material in this case. Second, it is possible that CI chondrites are not free of CAI material, with ≤ 2.5 wt% permitted by the data assuming the $\epsilon^{50}\text{Ti}$ value of pure CI material is not more negative than that of NC chondrites. Although rare, the aqueously altered remnants of a few CAIs have been identified

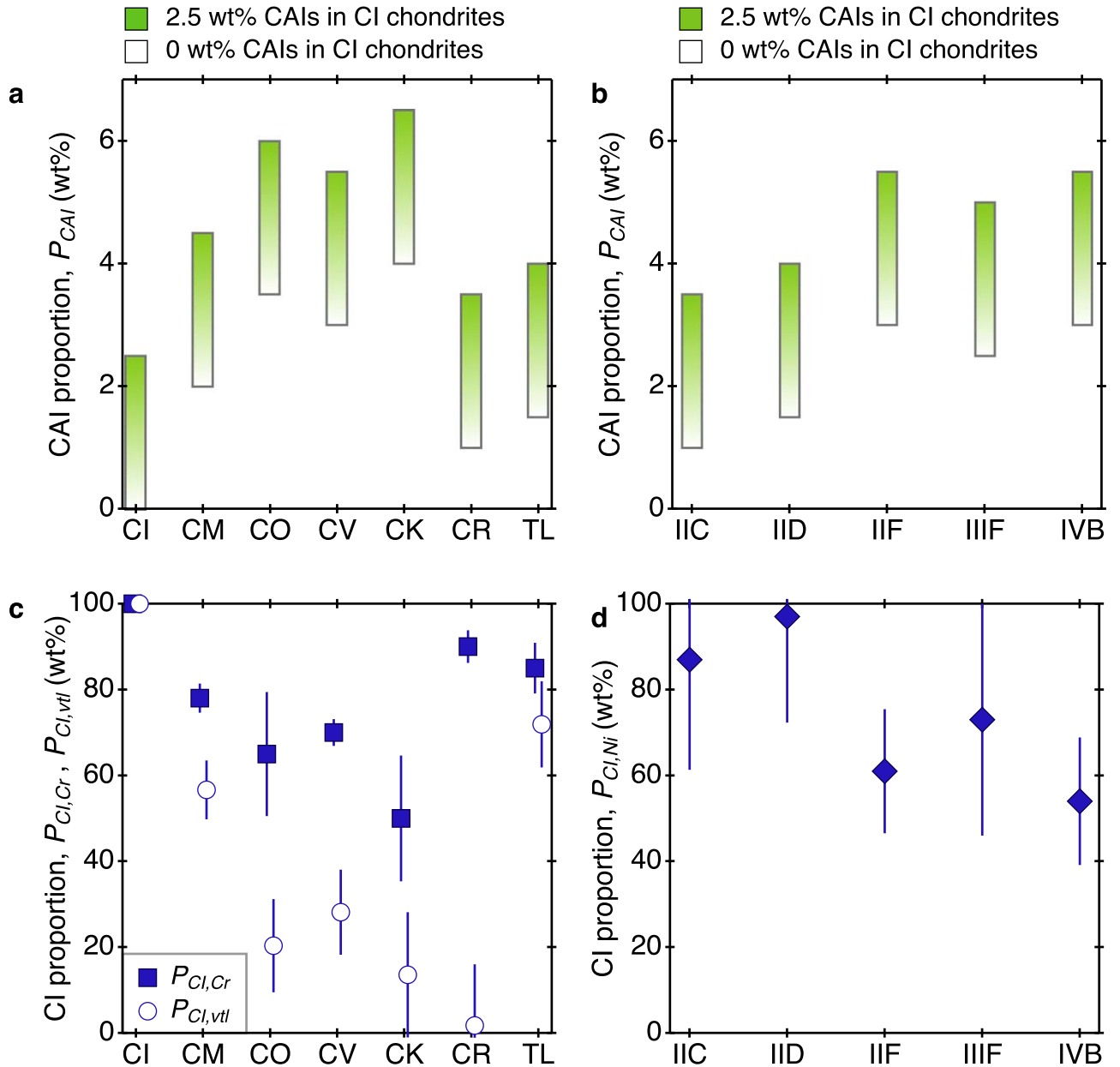


Figure 4. (a) Representative ranges of the proportions of CAI material (green) recovered from the mixing curves in Figure 2(c) for CC chondrite groups. The ranges in values (white-green vertical bars) result from the uncertainty regarding the amount of CAI material in CI chondrites (white: 0 wt%; green: 2.5 wt%). These ranges are very similar to those recovered from Figure 1. (b) The possible range of proportions of CAI material recovered from the mixing curves in Figure 2(d) for CC iron meteorite groups. (c) Representative proportions of CI material (blue) in CC chondrites recovered from Cr isotopic compositions in Figure 2(c) (squares) and from volatile element concentrations in Figure 3 (open circles). These values of $P_{CI,Cr}$ are very similar to those recovered from Figure 2(a). (d) The proportion of CI material in CC iron meteorites recovered from Figure 2(d). TL: Tagish Lake ungrouped chondrite.

in petrographic observations of CI chondrites (Frank et al. 2011; Gounelle & Zolensky 2014) and CAI material could also have been present in the matrix of CI chondrites in the form of dust grains from which CAIs formed. Additionally, the material collected from the comet Wild 2 during the NASA Stardust mission contains ~ 0.5 vol% bulk CAIs (Joswiak et al. 2017), which, combined with the observation of CAIs in every other CC chondrite group, argues that most planetary bodies that formed in the outer and distal regions of the protoplanetary disk contained at least a small amount of bulk CAIs (seemingly ≥ 0.5 wt%) as well as presumably some accompanying dust with a CAI isotopic composition. As such, in the likely scenario that CI chondrites contain close to ~ 2.5 wt% CAI material, pure CI material could have a very similar or identical

$\epsilon^{50}\text{Ti}$ and Ti/Si values to NC material. This would still be consistent with the isotopic and elemental concentration of CC chondrites being a mixture of NC, CAI, and CI material, albeit with CI material having a minimal or possibly nonexistent effect on the elemental and isotopic composition of refractory elements in CC chondrites. This possible range in the amount of CAI material in CI chondrites introduces an uncertainty into the amount of CAI material in the remaining CC chondrite groups that is typically larger than that calculated from the 2σ values of their measured isotopic compositions.

The proportions of CAI material recovered from Figures 2(c) and (d) in CC chondrites and iron meteorites, respectively, are shown in Figures 4(a) and (b) for CAI proportions in CI chondrites ranging from 0 to 2.5 wt%. The calculated CAI

proportions are very similar to those recovered by Burkhardt et al. (2019) for the case where CI chondrites contain 2.5 wt% CAI material and cover the same range of proportions as CC chondrites and iron meteorites. This result indicates that approximately the same amount of CAI material was present in the CC reservoir during its early evolution (to be present in CC iron meteorites, whose parent bodies accreted ~ 1 – 1.5 Myr after CAI formation; see Section 3.4) and late-stage evolution (to be present in all CC chondrites, whose parent bodies accreted between ~ 2 and 4 Myr after CAI formation; Sugiura & Fujiya 2014; Doyle et al. 2015). As such, CAI material appears to have existed in the CC reservoir at an approximately constant range of abundances for the majority of the disk’s lifetime (assuming the material in the CC reservoir dissipated at a similar time to the NC reservoir at ~ 3.8 – 4.8 Myr after CAI formation; Wang et al. 2017). The mineralogies, compositions, and isotopic signatures of CAIs strongly argue that these objects formed close to the young Sun (Wood 2004), implying that they migrated outwards from the location of their formation to be present in the CC reservoir. The refractory element isotopic compositions of CC iron meteorites demonstrate that this process must have occurred by the accretion ages of CC iron meteorite parent bodies (~ 1 – 1.5 Myr after CAI formation), arguing for outward migration speeds of these millimeter-sized objects in the young protoplanetary disk of $\gtrsim 2$ – 4 au Myr^{-1} (assuming that the barrier that separated the NC and CC reservoirs was located at ~ 2 – 4 au; Desch et al. 2018) within the first ~ 1 – 1.5 Myr of the disk. Moreover, this result argues that some millimeter-sized solids were able to persist in the disk for millions of years in the CC reservoir without spiraling inwards or being accreted into planetesimals.

3.3. The Proportions of CI Material in CC Chondrites

3.3.1. The Source of CI Material in CC Chondrites

The proportions of CI versus NC material in CC chondrites can be recovered from both their main component element isotopic compositions and plateau volatile element concentrations (Table 2 and Figure 4(c)). In all CC chondrite groups, $P_{\text{CI,vtl}}$ is systematically less than $P_{\text{CI,Cr}}$. This difference can be explained by the difference in $T_{c,50}$ between plateau volatile elements ($T_{c,50} < 800$ K) and main component elements (1300 K $< T_{c,50} < 1400$ K) and the effect that this has on the retention of these elements when material experiences elevated temperatures. Starting with plateau volatile elements, their low $T_{c,50}$ values (Wood et al. 2019) mean that these elements can have been lost easily from a chondrule when it was heated. This loss is reflected in the plateau volatile elemental compositions of chondrules, which are typically ~ 13 wt% that of matrix material (Hellmann et al. 2020). Additionally, the isotopic compositions of plateau volatile elements in chondrules differ significantly from those of the matrices of CC chondrites (e.g., the average $\delta^{66}\text{Zn}$ value for Allende chondrules is ~ 0.12 , while a matrix-rich sample is 0.35 ; Pringle et al. 2017), supporting different behaviors and retentions of these elements among chondrules and matrix (Van Kooten & Moynier 2019; Hellmann et al. 2020). As such, the value of $P_{\text{CI,vtl}}$ is expected to reflect the proportions of thermally processed material (chondrules and CAIs) and thermally unprocessed material (pristine matrix grains) in a given chondrite.

On the other hand, main component elements such as Cr and Ni have significantly higher $T_{c,50}$ values (Wood et al. 2019), and so are expected to have been lost minimally if at all when chondrules experienced elevated temperatures (Alexander 2019a). For instance, the elemental concentrations of Cr in chondrules and matrix differ by a factor of < 2 (Van Kooten et al. 2019), and so are much more similar than the concentration of plateau volatile elements in these components (chondrules contain ~ 13 wt% the concentration of these elements compared to the matrix; Hellmann et al. 2020). As such, the loss of these elements during chondrule formation is likely negligible and is not expected to be the dominant factor influencing the $P_{\text{CI,Cr}}$ and $P_{\text{CI,Ni}}$ values of a meteorite. Instead, trends in $P_{\text{CI,Cr}}$ and $P_{\text{CI,Ni}}$ likely reflect variations in the proportions of materials in the protoplanetary disk that originate from different nucleosynthetic sources (Dauphas et al. 2010; Qin et al. 2010; Sugiura & Fujiya 2014; Schneider et al. 2020). Dust and gas produced during different processes within supernovae and/or that were added at different times/locations to the protoplanetary disk could exhibit variations in their Cr isotopic compositions due to differences in the nucleosynthetic processes by which each of these generations of material were created. As such, the values of $P_{\text{CI,Cr}}$ and $P_{\text{CI,Ni}}$ likely reflect varying proportions of precursor materials from different sources. Interestingly, the isotopic compositions of main component elements among chondrules and matrix exhibit different behaviors in different chondrite groups. For instance, the $\epsilon^{54}\text{Cr}$ values of six individually extracted OC chondrules are comparatively tightly clustered with an average value (-0.29 ± 0.31 ; Schneider et al. 2020) that is indistinguishable from the bulk composition of these meteorites ($\epsilon^{54}\text{Cr} \sim -0.4$; Table 1). On the other hand, the measured $\epsilon^{54}\text{Cr}$ values of chondrules extracted from multiple CV chondrites effectively span the range of values from CI chondrites to bulk NC chondrites (i.e., $-0.79 < \epsilon^{54}\text{Cr} < 2.01$ for CV chondrites; Olsen et al. 2016; Schneider et al. 2020; Williams et al. 2020). Combined with the O and Ti isotopic compositions of individual chondrules extracted from CV chondrites, these values have recently been used to argue that some chondrules in CC chondrites in fact exhibit NC-like isotopic compositions (Williams et al. 2020). Interestingly, relict chondrule olivines (crystals from a previous generation of chondrules that did not fully melt during more recent chondrule remelting events) that contain nanometer-scale iron grains regularly display NC-like O isotopic compositions (Schrader et al. 2020). This observation argues that the precursor to CC chondrules could have been preexisting NC chondrules and that these CC chondrules adopted their isotopic compositions through the incorporation of CI material into NC chondrules when they experienced remelting and were able to exchange material with the dust and gas in their local region of the protoplanetary disk. The average $\epsilon^{54}\text{Cr}$ value of hundreds of pooled chondrules extracted from the Allende CV chondrite is ~ 0.58 (Schneider et al. 2020). This value is lower than the average typically recovered from individual extracted chondrules (e.g., ~ 0.84 ; Schneider et al. 2020) as well as the bulk value of CV chondrites of ~ 0.87 (Table 1), indicating that, on average, chondrules from CV chondrites contain a smaller proportion of CI material than CV matrix material. This result is consistent with the measured $\epsilon^{54}\text{Cr}$ value of the CV matrix of ~ 1.06 (note that this value is still lower than the measured value from CI chondrites; Schneider et al. 2020). The average $\epsilon^{54}\text{Cr}$ value of nine individual chondrules extracted from the Ornans CO chondrite is ~ 0.82

(Zhu et al. 2019), similar to the bulk $\varepsilon^{54}\text{Cr}$ of these meteorites of ~ 0.77 (Table 1). However, it is worth noting that the $\varepsilon^{54}\text{Cr}$ values measured from individual extracted CV chondrules argue that the process of extracting and measuring the isotopic signature of CC chondrules can yield higher $\varepsilon^{54}\text{Cr}$ values than that measured from hundreds of pooled chondrules. These higher values may result from the comparative ease in measuring the isotopic compositions of individual large chondrules compared to small chondrules (because they contain more Cr atoms), which could have grown to their large size by incorporating more CI material. As such, the actual representative average $\varepsilon^{54}\text{Cr}$ value of chondrules from CO chondrites may be lower than the values measured from the individual extracted chondrules. Additionally, the average $\varepsilon^{54}\text{Cr}$ value of 13 chondrules extracted from the Jbilet Winselwan CM chondrite is ~ 0.63 (Zhu et al. 2019), which is similar to the values measured from the pooled chondrules extracted from Allende and less than the bulk $\varepsilon^{54}\text{Cr}$ of the CM chondrites of ~ 1.02 (Table 1). Finally, the $\varepsilon^{54}\text{Cr}$ values of a number of chondrules extracted from CR chondrites have also been measured (Olsen et al. 2016; Van Kooten et al. 2016; Schneider et al. 2020). These values are typically far less variable than those recovered from chondrules from CV, CO, and CM chondrites and have an average value of ~ 1.44 , which is slightly higher than the bulk value for these meteorites of ~ 1.31 (Table 1).

Given the different sources of the variations in $P_{\text{CI,vtl}}$ compared to $P_{\text{CI,Cr}}$ and $P_{\text{CI,Ni}}$, the values of $P_{\text{CI,vtl}}$ are not expected to relate to $P_{\text{CI,Cr}}$ and $P_{\text{CI,Ni}}$ in the case where CC chondrites form through the mixture of dust populations from two different sources (i.e., NC and CI dust) from which chondrules subsequently formed (i.e., the mass fraction of chondrules is not expected to depend on the proportions of NC and CI dust). On the other hand, all three of these values, as well as the mass fraction of the matrix, are expected to be related to each other in the case where CC chondrites formed through the mixture of bulk NC chondrite material with CI dust because the volatile element concentration, the main component isotopic concentrations, and the mass fraction of matrix will all depend on the amount of this dust mixed into the meteorite. As such, the origin of the CI component in CC chondrites can be assessed by determining whether their values of $P_{\text{CI,Cr}}$, $P_{\text{CI,vtl}}$, and matrix mass fraction follow the expected trends for mixing between bulk reaccrionary NC chondrite material and CI dust. The mathematical details of such a mixing model are presented in the Appendix. This model predicts that

$$P_{\text{CI,Cr}} \approx \frac{\chi - \gamma}{1 - \gamma} + (1 - \chi)\beta, \quad (5)$$

where χ is the mass fraction of the matrix in a given CC chondrite, γ is the mass fraction of the matrix in an NC chondrite, and β is the average proportion of CI material incorporated into CC chondrules in a given group. This mixing model also predicts that

$$P_{\text{CI,vtl}} = \frac{\chi - \gamma}{1 - \gamma}. \quad (6)$$

As such,

$$P_{\text{CI,Cr}} \approx P_{\text{CI,vtl}} + (1 - \chi)\beta \quad (7)$$

and the difference in the proportions of CI material recovered from the Cr isotopic compositions and the plateau volatile

elemental concentrations, $\Delta P_{\text{CI}} = P_{\text{CI,Cr}} - P_{\text{CI,vtl}}$, is

$$\Delta P_{\text{CI}} \approx (1 - \chi)\beta. \quad (8)$$

The values of χ can be calculated from the volume fractions of the matrix identified from petrographic observations of CC chondrites (see the Appendix). The extent of aqueous alteration and metamorphism experienced by CK chondrites makes it difficult to identify reliably the volume fraction of the matrix in this group (Noguchi 1993; Braukmuller et al. 2018). Due to this uncertainty, we chose not to include CK chondrites in our discussion of mixing in this study (Hellmann et al. 2020).

The CV, CO, CM, and TL chondrites all exhibit the same clear linear relationships between $P_{\text{CI,Cr}}$, $P_{\text{CI,vtl}}$, and ΔP_{CI} with χ that matches the predicted values calculated using previously measured compositions of individual components of chondrites (Figures 5(a)–(c)). This behavior argues that the elemental and isotopic compositions of the main component and plateau volatile elements in these groups are related, so the compositions of these elements in CC chondrites originate from mixing bulk NC chondrite material and CI dust. Additionally, this single linear relationship indicates that chondrules in CV, CO, CM, and TL chondrites all share very similar Cr isotopic compositions (i.e., CV, CO, CM, and TL chondrites can be fit using a single value of $\beta \approx 0.57$; Figure 5(c)) and plateau volatile element concentrations (Hellmann et al. 2020).

Moreover, this model predicts that

$$I_{\text{CC},m}C_{\text{CC},m} = \frac{(\chi - \gamma)I_{\text{CI}}C_{\text{CI}} + \gamma(1 - \chi)I_{\text{NC},m}C_{\text{NC},m}}{\chi(1 - \gamma)}, \quad (9)$$

where $I_{\text{CC},m}$ and $C_{\text{CC},m}$ are the Cr isotopic and elemental concentrations of the matrix in CC chondrites, respectively, I_{CI} and C_{CI} are the bulk Cr isotopic and elemental concentrations in CI chondrites, respectively, and $I_{\text{NC},m}$ and $C_{\text{NC},m}$ are the Cr isotopic and elemental concentrations of the matrix in NC chondrites, respectively. Although the Cr isotopic composition of the complete CC matrix assemblage has only been measured for the Allende CV chondrite (Schneider et al. 2020), its value of $P_{\text{CI},m}$ (calculated using $C_{\text{CC},m} = 3100$ ppm; Rubin & Wasson 1987) is very close to that predicted by Equation (9) (Figure 5(d)), further supporting the idea that the main component and plateau volatile element compositions of CC chondrites originate from the mixture of bulk NC chondrite material and CI dust. This variation in $P_{\text{CI},m}$ with χ is consistent with the measured isotopic composition of the matrix regularly being less than CI values (Clayton & Mayeda 1999; Schrader et al. 2014; Pringle et al. 2017; Kadlag et al. 2019; Van Kooten & Moynier 2019; Schneider et al. 2020) and means that the matrix is not expected to display CI isotopic compositions for a general CC chondrite (only in the case where a chondrite is 100 wt% matrix, i.e., the CI chondrites). Note that amorphous silicates found in the matrix may have formed when microscopic droplets broke off from chondrules when they were molten (Dobrica & Brearley 2020). Due to their high-temperature origin, these droplets may be volatile-depleted compared to pristine matrix grains, possibly explaining why the measured elemental concentrations of plateau volatile elements in the matrix can sometimes be less than the CI value (Bland et al. 2005; Van Kooten et al. 2019).

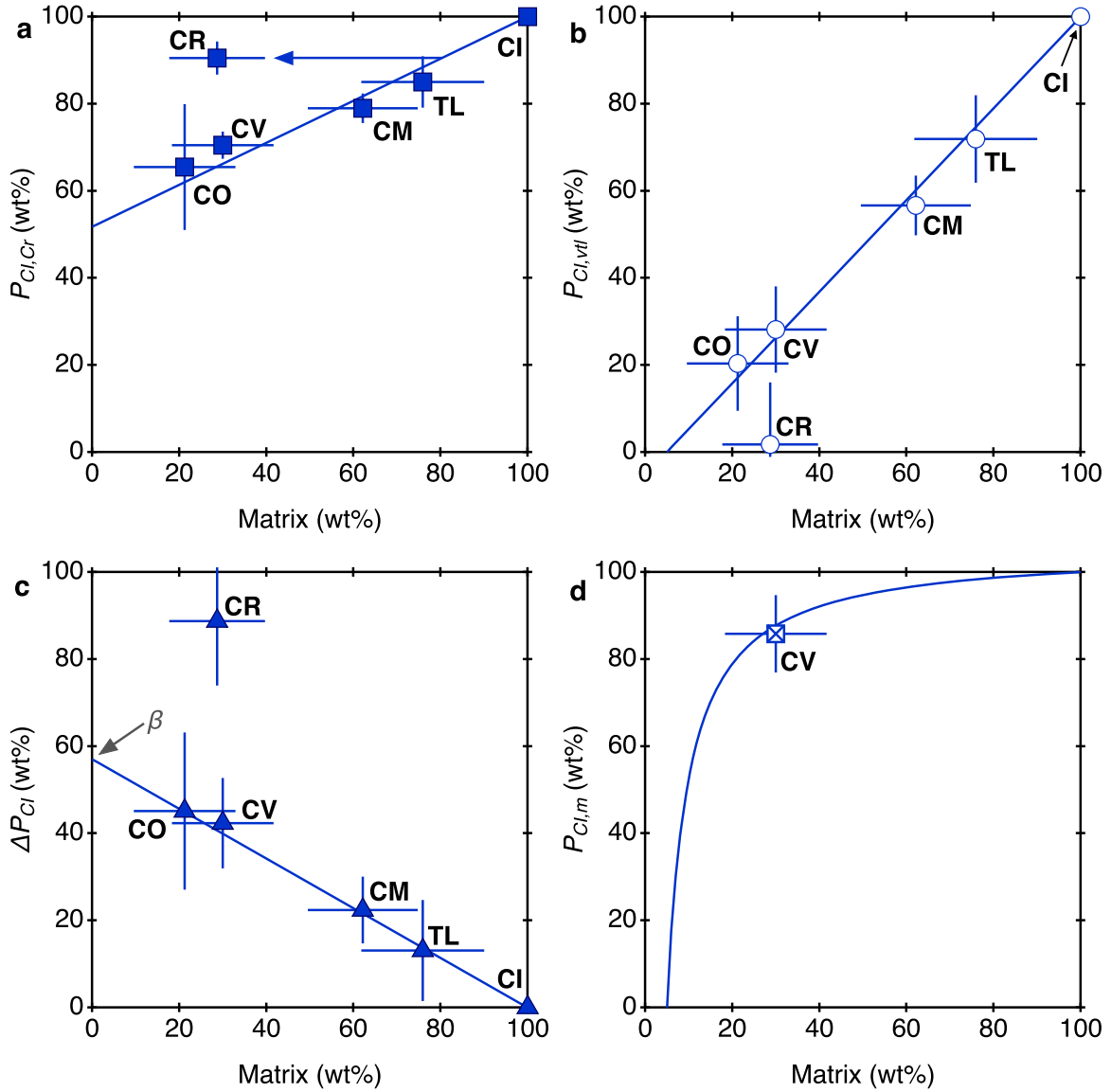


Figure 5. (a) Values of $P_{CI,Cr}$ as a function of matrix wt% for each CC chondrite group. The line is Equation (5) with $\beta = 0.57$ and $\gamma = 0.05$. The CR chondrites appear to have originally contained ~ 80 wt% matrix and a considerable portion of this material was transformed into chondrules through a different mechanism to that which generated chondrules in CO, CV, CM, and TL chondrites (blue arrow). (b) Values of $P_{CI,vlt}$ as a function of matrix wt% for each CC chondrite group. The line is Equation (6). (c) Values of ΔP_{CI} as a function of matrix wt%. The line is Equation (8). (d) The value of $P_{CI,m}$ for CV chondrite matrix. The line is Equation (9) in terms of P_{CI} .

3.3.2. The Consequences of the Proportions of CI Material in CC Chondrites

The linear relationships between $P_{CI,Cr}$, $P_{CI,vlt}$, and ΔP_{CI} with χ as well as the identification of very similar average proportions of CI material in chondrules in CV, CO, CM, and TL chondrites helps to elucidate the timing and environment in which these spherules formed. Chondrules in OC chondrites display relatively homogeneous Cr isotopic compositions with an average value that is indistinguishable from that of the bulk composition of these meteorites (Schneider et al. 2020). This relationship indicates that the matrix in these meteorites must also share the same average isotopic composition as chondrules (considering that the matrix and chondrules are the two predominant components of the bulk Cr isotopic composition of a chondrite). This observation is supported by the average O (Kita et al. 2010) and Ti (Gerber et al. 2017) isotopic compositions of chondrules in NC chondrites, which are also

indistinguishable from the bulk isotopic compositions of these meteorites. Assuming that NC-like chondrules originally formed through the melting of clumps of dust with NC-matrix-like isotopic compositions, this similarity in isotopic compositions between matrix and chondrules argues that chondrule formation did not cause the Cr isotopic composition of chondrules to change from that of the local dust and gas. Assuming this idea extends to CC chondrites, the differences in the average Cr isotopic compositions of chondrules in CV, CO, CM, and TL chondrites and the bulk isotopic compositions of these meteorites argue that these chondrules did not form from the dust and gas that existed in the local regions of the protoplanetary disk in which the parent bodies of these chondrites accreted (Schneider et al. 2020). Moreover, in the model framework where CC chondrites are mixtures of bulk preaccretionary NC chondrites and CI dust, the formation of chondrules in these regions of the disk would have decreased

the values of χ in CC chondrites without changing their average $P_{\text{CI,Cr}}$ values, causing the points in Figures 5(a)–(c) to no longer fall on the same straight lines. Together, both of these observations argue that new CV, CO, CM, and TL chondrules did not form in the CC reservoir. Instead, the O isotopic composition of relict grains (Schrader et al. 2020) and the abundance of chondrules among different CC chondrite groups coupled with their isotopic compositions (Figure 5) argue that chondrules found in these CC chondrites were originally NC-like chondrules that adopted their current isotopic compositions when they were remelted and were able to incorporate CI material from their local dust and gas. During this process, these chondrules appear to have been able to adopt a spectrum of isotopic compositions ranging essentially from that of NC chondrules to CI material, presumably depending on the varying extent of incorporation of CI material experienced by each individual chondrule (Olsen et al. 2016; Schneider et al. 2020; Williams et al. 2020). Our observation of very similar average proportions of CI material in chondrules in CV, CO, CM, and TL chondrites argues that these objects incorporated the same average amount of CI material from their surrounding dust and gas in all of these groups. This result indicates that the remelting of NC chondrules to form CC chondrules in CV, CO, CM, and TL chondrites must have all occurred in the same environment in the protoplanetary disk (i.e., in an environment with a single average P_{CI} value) rather than the isotopically different environments in which their parent bodies accreted (evidenced by the different bulk isotopic compositions of CC chondrites). CC chondrules also appear to have exchanged refractory elements with the local dust and gas when they were molten such that they adopted an increased CAI proportion compared to chondrules in NC chondrites (Gerber et al. 2017).

A number of recent measurements have argued that the parent asteroids of CI chondrites and meteorites with isotopic signatures similar to CI chondrites (e.g., the TL and WIS 91600 chondrites; Brown et al. 2000; Choe et al. 2010; Herd et al. 2012) formed in the distal solar system (Gounelle et al. 2008). These measurements include the refractory element concentrations of CI chondrites (which argue that these meteorites originate from $\gtrsim 15$ au; Desch et al. 2018), the isotopic compositions of carbonates in TL (which link TL with comets; Fujiya et al. 2019), and the paleomagnetic remanences of TL and WIS 91600 (which argue that these meteorites originate from $\gtrsim 10$ au; Bryson et al. 2020a, 2020b). A gradient in the amount of CI material existed throughout the CC reservoir (evidenced by the different bulk Cr isotopic compositions among CC chondrites), arguing either that distal CI dust migrated inwards and polluted a region of the disk that originally had a composition matching NC + CAI material to create the CC reservoir, or that NC + CAI dust migrated outwards and polluted a region of the disk that originally had a CI composition to generate the CC reservoir. In either of these cases, the result will have been a mixture of NC, CAI, and CI material, with an increasing amount of CI material at larger heliocentric distances. Because of this spatial variation in P_{CI} , the very similar average values of P_{CI} recovered from chondrules in CV, CO, CM, and TL chondrites argue that the environment in which NC chondrules remelted to form CC chondrules had a limited spatial extent, indicating that chondrule remelting occurred only in a restricted region of the CC reservoir. Given the low value of $P_{\text{CI,Cr}}$ in chondrules in CV, CO, CM, and TL chondrites compared to the bulk values

recovered from these meteorites (Figure 5(a)), chondrule remelting appears to have occurred relatively proximally within this reservoir. A pressure maximum has been proposed to have existed in the disk just outside of the feature that introduced the NC–CC dichotomy (i.e., at the innermost extent of the CC reservoir; Brasser & Mojzsis 2020), suggesting that chondrule remelting could be associated either with this pressure variation itself or the feature that introduced this pressure maximum.

Within the framework of CC chondrule remelting over a limited region that was relatively proximal in the CC reservoir, there are then two possible scenarios by which bulk CC chondrites could have been generated. First, it is possible that these newly remelted CC chondrules and some of the dust in the chondrule remelting region were redistributed outwards from this region where they mixed with additional CI dust in varying proportions to produce bulk CC chondrites (Figure 6(d)). Such outward migration of millimeter-sized objects has been proposed to have occurred efficiently in the midplane of the disk (Ciesla 2007, 2009) and has been invoked to explain the presence of CAI- and chondrule-like objects in the fragments of the comet Wild 2 collected during the NASA Stardust mission (Brownlee et al. 2006) as well as CAIs and chondrules with CC-like O isotopic composition in the TL and WIS 91600 chondrites (Russell et al. 2010; Yamanobe et al. 2018; Bryson et al. 2020a, 2020b; Ushikubo & Kimura 2021). Second, it is possible that CI dust migrated inwards over time and gradually piled up in the inner extent of the CC reservoir against the barrier that introduced the NC–CC dichotomy. The inward motion of material in protoplanetary disks is supported by surplus luminosity measurements of Sun-like stars in their disk phases, which indicate that material from these disks is actively moving inwards and being accreted onto the star (Hartmann et al. 1998). Additionally, pebble accretion models argue that objects with sizes on the order of millimeters to centimeters (e.g., larger chondrules, unmelted clumps of dust) are expected to have drifted inward as they experienced a headwind due to gas drag (Lambrechts & Johansen 2014). In this case, CC chondrite parent bodies could have accreted in the same region that CC chondrules were remelted because the composition of the gas and dust in this region is expected to have evolved toward the CI value over time due to this inward migration, consistent with proposals that the pressure maximum at this location facilitated planetesimal formation (Morbidelli 2020). Given this possible temporal evolution of P_{CI} in this region, the similarity in recovered CI proportions in chondrules from CV, CO, CM, and TL chondrites argue that these solids must have all adopted their Cr isotopic signatures not only within a restricted region of the disk but also at very similar times, favoring a localized event causing the remelting of chondrules in CV, CO, CM, and TL chondrites rather than ongoing phenomena such as planetary motion, bow shocks, nebula lightning, etc., that are expected to have produced chondrules continuously over the lifetime of the disk. The timing of chondrule remelting is a topic of uncertainty, with Pb–Pb dating of individual chondrules producing a broad range of ages that span ~ 0 –4 Myr after CAI formation for individual chondrules from OC, CV, and CR chondrites (Bollard et al. 2017; Connelly et al. 2017; Bollard et al. 2019), while Al–Mg and Hf–W dating produce narrower time intervals that overlap within uncertainties for CV and CO chondrules at ~ 2 –2.5 Myr after CAI formation (Kruahashi et al. 2008;

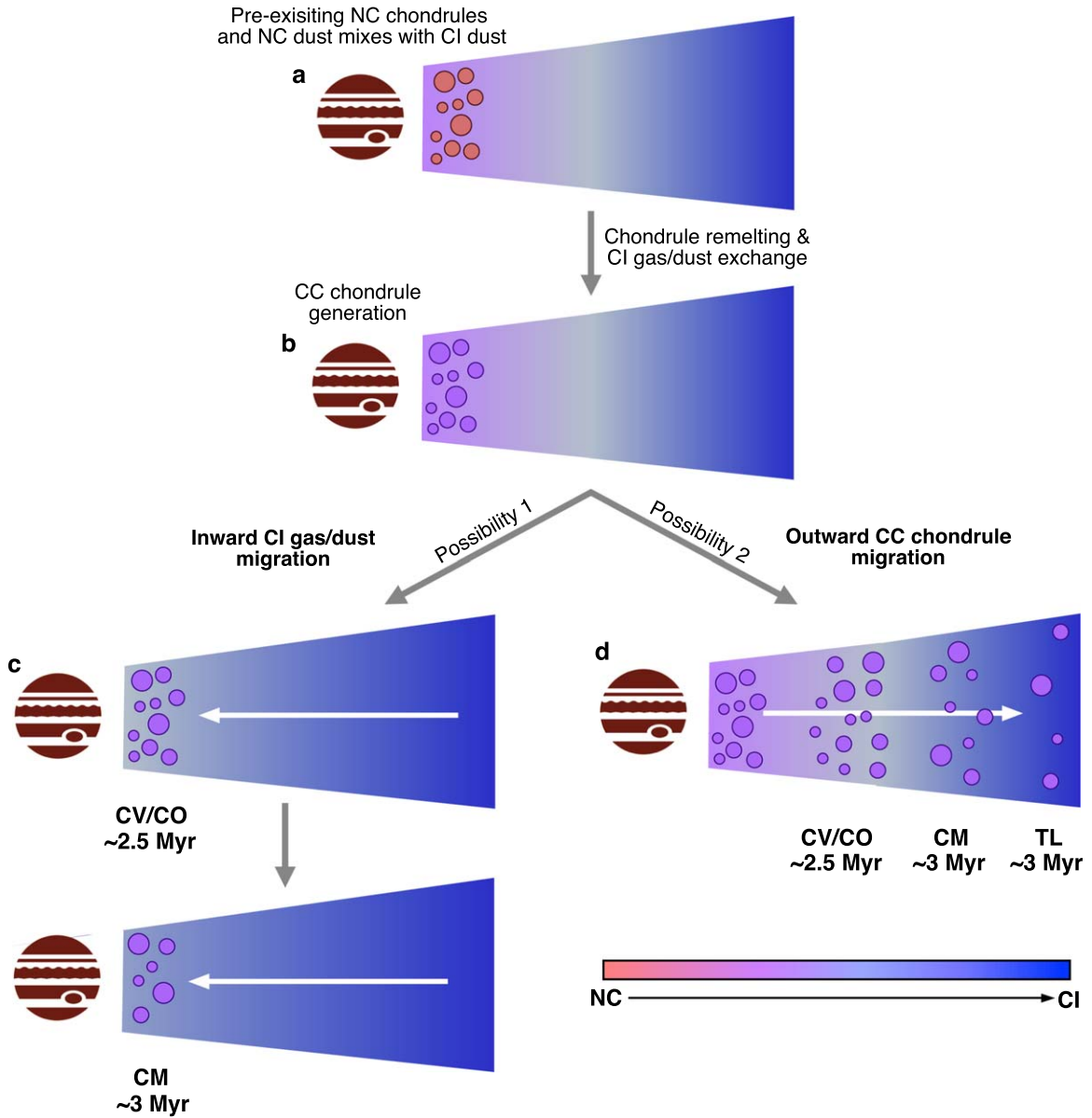


Figure 6. Schematic showing the potential isotopic and spatial evolutions of chondrules throughout the CC reservoir. Red represents NC material, dark blue represents CI material, and pink through light blue to dark blue represent a mixture of NC and CI material with increasing CI proportion. The feature causing the NC–CC dichotomy is nominally indicated by Jupiter. Chondrules are shown as circles of different sizes. (a) Preexisting NC-like chondrules coexist with a mixture of NC and CI gas and dust prior to being remelted. (b) NC chondrules remelt and exchange Cr with their local gas and dust when they incorporate CI material to produce CC chondrules. (c) One possible subsequent isotopic evolution where CI dust migrates inwards (white arrow), polluting the chondrule remelting region and increasing its P_{CI} value. The CC chondrite parent bodies then accrete from this mixture of chondrules and dust at different times. (d) A second possible subsequent evolution where CC chondrules and some accompanying dust are redistributed outwards (white arrow) from the chondrule formation region and mix with increasing amounts of CI dust to produce reservoirs from which the different CC chondrite parent bodies accreted. The proposed formation distances of CC chondrite parent bodies (Desch et al. 2018; Bryson et al. 2020a, 2020b) suggest that both of these models occurred in the disk.

Schrader et al. 2017; Pape et al. 2019; Gregory et al. 2020) and yield a second distinct and narrow interval for CR chondrules at ~ 3.7 Myr after CAI formation (Nagashima et al. 2014; Budde et al. 2018). As such, Al–Mg and Hf–W ages are consistent with a single CC chondrule remelting event (or possibly multiple repeated events over a short time interval, possibly up to ~ 0.5 Myr) for CV, CO, CM, and TL chondrites, although a systematic and reliable set of chondrule remelting ages from all of these groups are required to assess whether this was certainly the case. Both the outward chondrule redistribution model and the inward CI dust migration model produce an isotopic composition of the matrix in CC chondrites that evolves toward CI values over time, a reduction in the relative

amount of chondrules through dilution of bulk NC chondrite material by CI dust over time, and maintains the same chondrule isotopic signature among CV, CO, CM, and TL chondrites, recreating all of the experimental observations (Figure 7). Given the proposed formation distances of CC chondrite parent bodies (i.e., the CO, CM, and CV parent bodies accreted between ~ 3 –4 au, and the CI and TL parent bodies accreted at >10 au; Desch et al. 2018; Bryson et al. 2020a, 2020b), it appears that both of these processes potentially acted contemporaneously in the disk, with the net inward migration of dust, gas, and pebbles into the CC chondrule remelting region being the possible explanation for the origin of the compositions of general CC chondrites (CV,

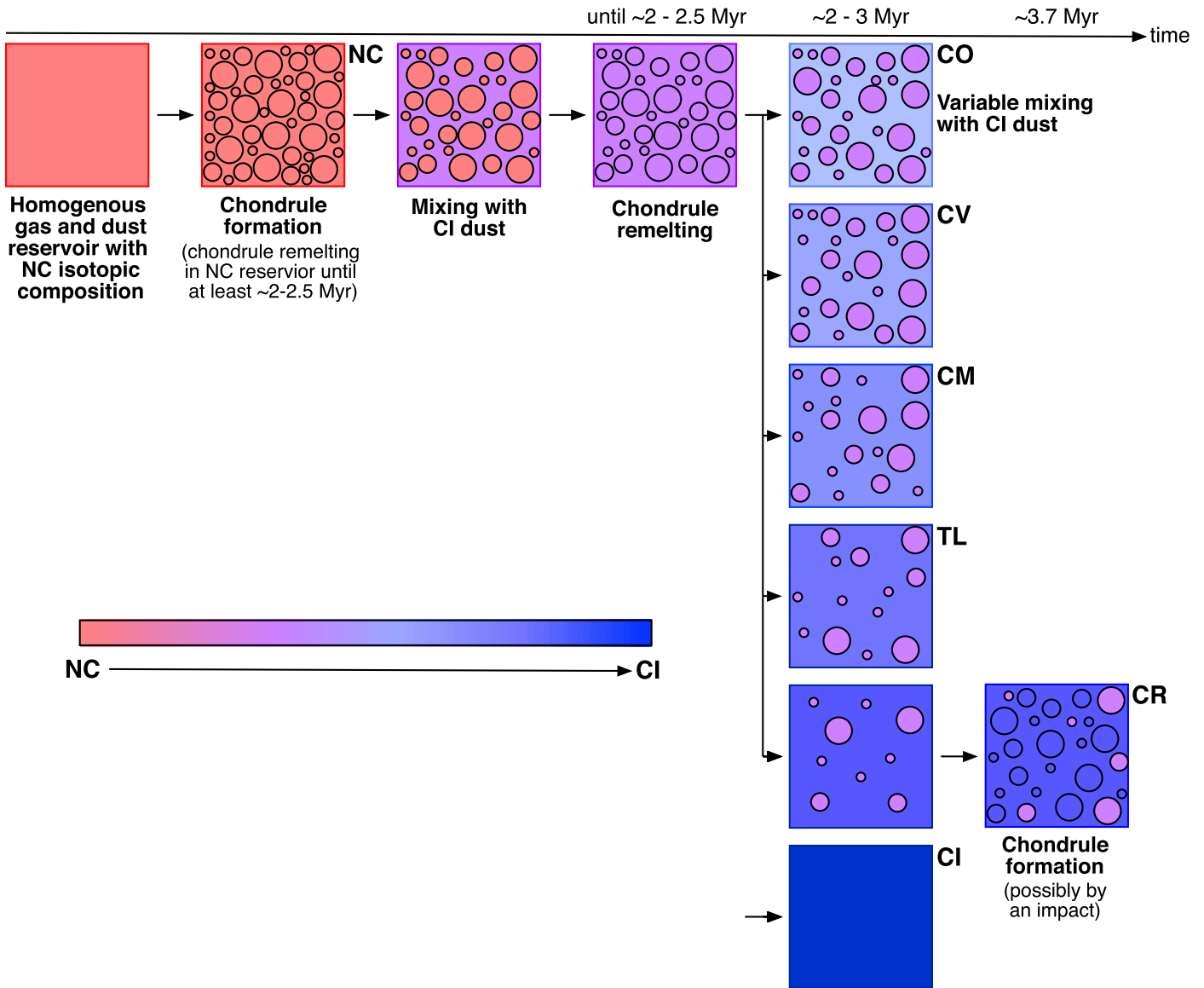


Figure 7. Schematic showing the evolution of CC chondrite Cr isotopic compositions. At early times, dust with an NC-like isotopic composition (red) existed and a considerable portion of this material formed chondrules (circles). After this event, CI dust pollutes this material, increasing the proportion of CI material in the dust (pink) and diluting chondrules. These chondrules are then remelted when they exchanged Cr with the surrounding dust and gas, adopting an average Cr isotopic composition that matches that of the dust and gas. Additional CI material is then added to this mixture of dust and chondrules in varying proportions (further diluting chondrules) to create bulk CO, CV, CM, and TL chondrites (increasing intensity of blue colors in the dust component). Finally, at ~ 3.7 Myr after CAI formation, some of the dust in the CR reservoir transforms into chondrules, possibly due to melting caused by an impact between two asteroid-sized bodies, one of which was originally matrix rich (~ 80 wt%). It is possible that some chondrules with isotopic compositions that match those in CO, CV, CM, and TL chondrites could still persist in the CR chondrites (pink circles), although the measured isotopic compositions of chondrules in CR chondrites argue that most of these solids were formed through the relatively late melting of matrix (dark blue circles). All times are millions of years after CAI formation.

CO, and CM chondrites; Figure 6(c)), and the outward migration of chondrules possibly explaining the compositions of TL, WIS 91600, and potentially comets (Figure 6(d)).

Notably, CR chondrites fall off the expected trends in Figure 5. Starting with their Cr isotopic composition, CR chondrites exhibit significantly higher $\varepsilon^{54}\text{Cr}$ values than the value predicted from Equation (5) using their observed proportion of matrix (~ 30 wt%). Unlike CV, CO, CM, and TL chondrites, this signature suggests that the Cr isotopic composition of CR chondrites is not a simple mixture of bulk NC chondrite material and CI material, and instead, that some of the original matrix in CR chondrites was transformed into chondrules. This observation is consistent with the measured elemental compositions of chondrules and matrix in CR

chondrites, which have been used to argue that these constituents formed through a different mechanism to those in CM and CV chondrites (Van Kooten et al. 2019). One possible process that could have transformed the matrix into chondrules was an energetic impact between asteroid-sized bodies (Johnson et al. 2015). This mechanism has been proposed as the origin of chondrules in CB chondrites (Krot et al. 2005), which share a number of structural, compositional, and isotopic similarities with CR chondrites (Krot et al. 2002). In this case, a body that was predominantly matrix (~ 80 wt%) could have been impacted, causing a significant portion of this material to have melted and been ejected into space where it solidified to produce new chondrules that then accreted with any micrometer-scale material that existed in this region of the

protoplanetary disk (which could be a mixture of unprocessed dust grains in the local region of the disk and any microscopic material created by the impact) to form the new CR chondrite parent body (Figure 7). This chondrule generation mechanism is also consistent with the much narrower range of individual chondrule $\epsilon^{54}\text{Cr}$ values observed among CR chondrites (1.13 to 1.72; Olsen et al. 2016; Van Kooten et al. 2016; Schneider et al. 2020) compared to CV chondrites (−0.79 to 2.01; Olsen et al. 2016; Schneider et al. 2020; Williams et al. 2020), and also explains why the individual CR chondrule isotopic compositions are much more similar to the bulk value of these chondrites compared to CV chondrites. This departure from the trends exhibited by CO, CV, CM, and TL chondrites also argues that chondrules in these groups were not formed by the same mechanism as that which generated CR chondrules.

Considering the plateau volatile element concentration of CR chondrites, a handful of these meteorites (e.g., GRO 95577, Al Rais, Renazzo; Bland et al. 2005) display relatively high concentrations of these elements (~ 60 wt% that of CI chondrites as opposed to ~ 10 wt% that of CI chondrites in most CR chondrites; Wiesberg & Huber 2007; Figure 3) and high matrix proportions (up to 60–70 vol%; Schrader et al. 2011), although the majority of these meteorites are significantly depleted in plateau volatile elements compared to CV and CO chondrites (which exhibit similar matrix mass fractions to most CR chondrites; Figures 3 and 5). This observation argues that CR chondrites underwent additional volatile loss compared to CV, CO, CM, and TL chondrites, consistent with a different formation history for the constituents of CR chondrites. Based on an impact origin for CR chondrites, it is possible that this event produced abundant micrometer-scale silicate melt droplets, which could have lost volatile elements because they were thermally processed and have made their way into the matrices of these meteorites. As such, these meteorites could contain a volatile-depleted matrix as well as chondrules that are potentially more volatile-depleted than those in CV, CO, CM, and TL chondrites due to their different formation mechanism. This scenario is supported by Figure 5(b) and could be explored by future measurements. Importantly, petrographic observations of CR chondrites demonstrate that their matrices contained water ice (Schrader et al. 2014) and still contain presolar grains (Davidson et al. 2019b), identifying that a primitive, unprocessed component was present in the reservoir from which these meteorites accreted. Interestingly, CR chondrites with higher plateau volatile element concentrations (i.e., those that contain a higher proportion of CI material such as GRO 95577, Al Rais, and Renazzo, as evidenced by their higher matrix proportions; Bland et al. 2005; Wiesberg & Huber 2007) also display higher degrees of aqueous alteration (Schrader et al. 2014), suggesting that water ice in CC chondrites is linked with the proportion of CI material within these meteorites. This relationship also holds for CO and CM chondrites, the former of which exhibits lower $P_{\text{CI,vil}}$ and $P_{\text{CI,Cr}}$ values (Figure 4(c)) and shows minimal evidence of parent body aqueous alteration (Alexander et al. 2018a; Davidson et al. 2019a), while the latter of which contain higher $P_{\text{CI,vil}}$ and $P_{\text{CI,Cr}}$ values (Figure 4(c)) and show numerous lines of evidence that they experienced extensive aqueous alteration on their parent body (Rubin et al. 2007; Alexander et al. 2013; Howard et al. 2015). As such, the volatile budget of a CC chondrite appears to reflect its P_{CI}

value, arguing for a CI-like origin for much of the volatile content of these meteorites.

3.4. The Proportions of CI Material in CC Iron Meteorites

The proportions of CI material in CC iron meteorites recovered from their Ni isotopic compositions occupy a very similar range (54–97 wt%) to those recovered from the Cr isotopic compositions of CC chondrites (50–90 wt%; Table 2, Figure 4). Much like the recovered CAI proportions in CC chondrites and iron meteorites, this behavior indicates that CC iron meteorites contain a similar abundance of CI material as CC chondrites and that this can be a considerable portion of the material in these meteorites.

Due to differences in the accretion ages of their parent asteroids, the combined P_{CI} values from CC chondrites and iron meteorites represent a time-resolved record of the abundance of CI material throughout the CC reservoir. To recover this record, the timing of accretion of the CC meteorite parent bodies must be known. For CC chondrites, these times have been recovered from measured chondrule remelting ages (accretion must have occurred after the most recent chondrule remelting event) and from dating events on their parent bodies (e.g., metamorphism and/or aqueous alteration). These times span ~ 2.5 – 4.5 Myr after CAI formation for the different CC groups (Sugiura & Fujiya 2014; Doyle et al. 2015; Desch et al. 2018; Kleine et al. 2020). For CC iron meteorite parent bodies, these times can be calculated from their differentiation ages recovered from Hf–W dating of these meteorites (Kruijer et al. 2017). Differentiation can be modeled as having occurred once the temperature of a planetesimal reached ~ 1500 K when silicate melting had progressed to such an extent that molten metal was able to readily separate out from the semimolten silicate material under the influence of gravity and shear stresses resulting from convection (Bryson et al. 2019). The predominant source of internal heat in planetesimals was the radioactive decay of ^{26}Al (Hevey & Sanders 2006). As such, the Al concentration of the precursor chondrite-like material from which CC iron meteorites differentiated will have played a key role in setting the differentiation time recorded by these meteorites. Unfortunately, this concentration cannot be measured directly from these meteorites because Al is a lithophile and therefore did not partition appreciably into asteroid cores. However, it is possible to estimate this concentration from the P_{CAI} values recovered from iron meteorites. As shown in Figure 1, these values reflect the amount of refractory elements in the chondrite-like precursor that melted to produce CC iron meteorites, with higher values of P_{CAI} reflecting higher concentrations of Al in this material. From the trend in Figure 1, the ratio of the concentration of Al ($C_{\text{CC,Al}}$) to Si ($C_{\text{CC,Si}}$) in a bulk CC-like chondrite can be expressed as

$$\frac{C_{\text{CC,Al}}}{C_{\text{CC,Si}}} = \frac{C_{\text{NC,Al}}(1 - P_{\text{CAI}}) + C_{\text{CAI,Al}}P_{\text{CAI}}}{C_{\text{NC,Si}}(1 - P_{\text{CAI}}) + C_{\text{CAI,Si}}P_{\text{CAI}}}, \quad (10)$$

where $C_{\text{NC,Al}}$ (1.18 wt%; Alexander 2019b) and $C_{\text{CAI,Al}}$ (17.3 wt%; Stracke et al. 2012) are the Al concentrations in bulk NC chondrites and group 1 CAIs, respectively, and $C_{\text{NC,Si}}$ and $C_{\text{CAI,Si}}$ are the Si concentrations in bulk NC chondrites and group 1 CAIs, respectively (Table 1). We calculated $C_{\text{CC,Al}}$ using the values in Table 2 assuming that CI chondrites contain 2.5 wt% CAI material and using a nominal average $C_{\text{CC,Si}}$ value of 16 wt% (the Si concentration in CO chondrites, which contain low amounts of water and likely similar amounts of metal to the

Table 3

Calculated Al Concentrations in the Precursor Chondrite-like Material to CC Iron Meteorites, the Adopted Differentiation Times (t_d ; Kruijer et al. 2017) and Calculated Accretion Times (t_a) for CC Iron Meteorite Parent Bodies, and Adopted Representative Accretion Times of CC Chondrite Parent Bodies (Sugiura & Fujiya 2014; Doyle et al. 2015; Kleine et al. 2020)

	Calculated Al Concentration (wt%)	Adopted t_d (Myr after CAI Formation)	Calculated t_a (Myr after CAI Formation)
IIC	1.6	2.6	1.4
IID	1.6	2.3	1.3
IIF	1.9	2.5	1.5
IIIF	1.8	2.2	1.4
IVB	1.9	2.8	1.6
CO			2.5
CV			2.7
CM			3.25
TL			3.25
CR			3.7

material from which CC iron meteorites differentiated; Table 1). The calculated values of $C_{CC,Al}$ are included in Table 3. These values occupy the higher end of the range measured in CC chondrites (0.84–1.83 wt%; Alexander 2019a), which could be an artifact introduced by our method of calculating this value and would cause the recovered accretion ages to vary by up to ~ 0.2 Myr. However, this uncertainty will have affected all of the calculated ages similarly, such that the relative variations in our calculated CC iron meteorite parent body accretion ages (e.g., the IVB iron meteorites accreting at least ~ 0.3 Myr after the IID iron meteorites) are likely still reliable.

The amount of heat produced by the radioactive decay of ^{26}Al , h , at any given time after CAI formation can be expressed as

$$h = h_0 C_{CC,Al} \psi_{Al} \exp\left(-\ln(2) \frac{t}{\lambda}\right), \quad (11)$$

where h_0 is the heat production of ^{26}Al (0.355 W kg^{-1}), ψ_{Al} is the value of $^{26}\text{Al}/^{27}\text{Al}$ at the time of CAI formation (5.25×10^{-5}), t is time after CAI formation, and λ is the half-life of ^{26}Al decay (0.717 Myr; Bryson et al. 2019). Considering that chondritic material accreted at $T_a \approx 200 \text{ K}$ and had to heat up to $T_d \approx 1500 \text{ K}$ for efficient differentiation to occur, and assuming that asteroids accreted instantaneously and that there was minimal heat loss from the surface of the body within a few half-lives of ^{26}Al decay (Bryson et al. 2019), the temperature difference between the temperature of differentiation and the temperature of accretion can be expressed as

$$\frac{h_0 C_{CC,Al} \psi_{Al} \lambda}{C_p \ln(2)} \left(\exp\left(-\ln(2) \frac{t_a}{\lambda}\right) - \exp\left(-\ln(2) \frac{t_d}{\lambda}\right) \right) = T_d - T_a \approx 1300, \quad (12)$$

where C_p is the heat capacity of the chondritic material ($1300 \text{ J kg}^{-1} \text{ K}^{-1}$; Kruijer et al. 2017), t_a is the accretion time after CAI formation, and t_d is the measured time of differentiation after CAI formation. Our adopted value of C_p accounts for the increase in this parameter with temperature from the reference value measured at room temperature ($800 \text{ J kg}^{-1} \text{ K}^{-1}$) as well as the effects of latent heat introduced when material starts to

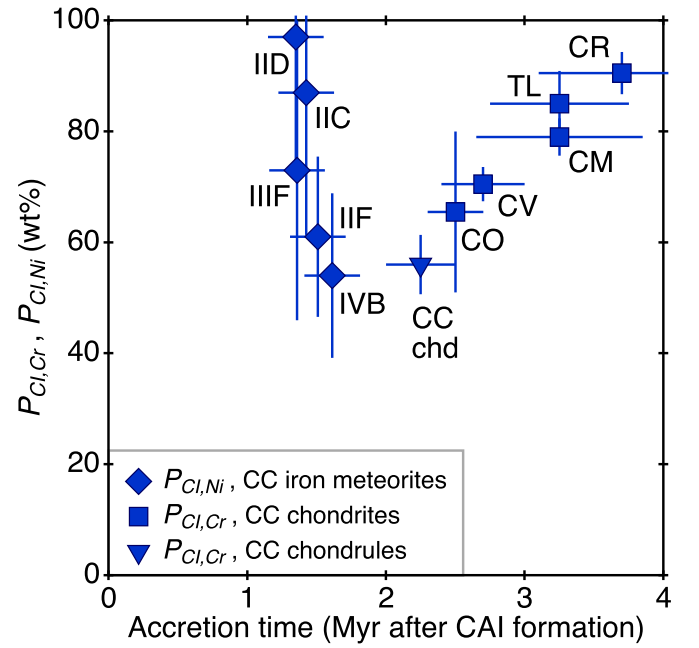


Figure 8. The evolution of P_{Ci} in the CC reservoir recovered from CC iron meteorites (diamonds), CC chondrites (squares), and CC chondrules (upside-down triangle; refers to chondrules in CO, CM, CV, and TL chondrites).

melt (Bryson et al. 2019). Taking t_d values from Kruijer et al. (2017), our calculated values of t_a range from 1.3–1.6 Myr after CAI formation (Table 3). Within this range, CC iron meteorite groups with larger $P_{Ci, Ni}$ values tend to have accreted at earlier times than CC iron meteorite groups with lower $P_{Ci, Ni}$ values (Figure 8), producing a steep decreasing trend in $P_{Ci, Ni}$ with the calculated parent body accretion time after CAI formation. Using representative values of parent body accretion ages presented by Sugiura & Fujiya (2014), Doyle et al. (2015), and Kleine et al. (2020; Table 3), the opposite trend exists among CC chondrites, where the younger parent bodies of these meteorites exhibit higher P_{Ci} values, producing a shallower increasing trend in $P_{Ci, Cr}$ with the calculated parent body accretion time after CAI formation (Figure 8). Note that the recovered $P_{Ci, Cr}$ from CR chondrites likely corresponds to earlier times than their calculated accretion times due to the possible impact origin of the constituents of this meteorite group that will have moved the accretion age of their parent body to later times.

It is worth noting that the typical uncertainties on the differentiation ages recovered from Hf–W dating of CC iron meteorites range from ~ 0.5 to >1 Myr (Kruijer et al. 2017), which is larger than the difference in parent body accretion ages that we calculate among these meteorites (~ 0.3 Myr; Table 3). As such, it is difficult to say with certainty that the steep trend in the $P_{Ci, Ni}$ values among these meteorites is real. Regardless of the existence of this trend, the $\epsilon^{62}\text{Ni}$ values of CC iron meteorites are distinct (Nanne et al. 2019), arguing that the parent bodies of these meteorites accreted differing amounts of CI material. Similarly to CC chondrites, this result supports variations in the time and/or location of the formation of their parent bodies within the CC reservoir. In the following discussion, we assume that the steep trend in $P_{Ci, Ni}$ among CC iron meteorites is real. Importantly, even in the case where this is not true, one of the two explanations proposed in the

following is likely still required to explain the distinct values of $P_{\text{Cl,Ni}}$ among CC iron meteorites.

The nominal change in the direction of P_{Cl} with time between CC iron meteorites and CC chondrites has potential implications regarding the origins and addition of material to the protoplanetary disk and the accretion of the first planetary bodies in the solar system. Based on refractory and main component element isotopic compositions, Burkhardt et al. (2019) and Nanne et al. (2019) propose that sequential generations of dust with distinct isotopic signatures were added to the protoplanetary disk. In this model, the solar nebula initially consisted of material with a CAI-like isotopic composition from which CAIs and the Sun formed. Shortly after the formation of these objects, these authors propose that dust with an NC isotopic signature could have been added to the disk close to the Sun that then drifted outwards, taking CAI material with it. This process led to a region near the Sun that was predominantly composed of this new material (i.e., the NC reservoir) and a region farther from the Sun that was a mixture of original and newer materials (NC + CAI material, i.e., the CC reservoir in the model proposed by Burkhardt et al. 2019 and Nanne et al. 2019; Kruijer et al. 2019; Brennecka et al. 2020; Kleine et al. 2020). Based on the findings of this study from nonrefractory elements, a third reservoir of material with elemental and isotopic compositions similar to CI chondrites also appears to have existed in the protoplanetary disk and a component of this reservoir was present throughout the CC reservoir in varying proportions over space and/or time. Interestingly, the isotopic compositions of refractory and main component elements in NC and CI material are much more similar to each other than either is to CAI material (Table 1). This observation suggests that both NC and CI dust could share a similar origin and so were possibly both added to the disk after the ignition of the Sun at potentially similar times. Because this CI reservoir is likely associated with the outer reaches of the protoplanetary disk (Section 3.1), CI material was more likely to have been added at larger heliocentric distances than NC material.

Based on our discussion in Section 3.3, this CI material was present throughout the CC reservoir in varying proportions. The time that this CI material reached the CC reservoir relative to NC material is currently unknown but has key implications regarding our interpretation of the trends in P_{Cl} values among CC iron meteorites and CC chondrites. In the case where CI material was in the CC reservoir before NC + CAI material, the initial isotopic composition of the CC reservoir would have been CI-like. The CC reservoir could then have been polluted by outwardly drifting NC + CAI material, reducing the P_{Cl} value of the CC reservoir over time (potentially captured by the evolution of P_{Cl} among CC iron meteorites). At some time, this apparent outward drift appears to have ceased and distal CI material then seemingly started making its way inward into the CC reservoir (Figure 6). This material could then have started piling up against the barrier that caused the NC–CC dichotomy, increasing the P_{Cl} values in the CC reservoir (captured by the evolution of P_{Cl} in CC chondrites). At a given heliocentric distance, this model produces an evolution of P_{Cl} that starts at CI values, before decreasing as NC + CAI material is added, and then finally increasing again as additional, distal CI material is introduced (Figure 9(a)). As such, this model involves a change in the direction of the predominant flow of material in the first ~ 10 au of the disk over time, from outward

between ~ 0 and 2 Myr after CAI formation to inward at $\gtrsim 2$ Myr after CAI formation. This model also implies that either the NC–CC barrier was introduced after the accretion ages of CC iron meteorites (~ 1 –1.5 Myr after CAI formation) such that outwardly drifting NC + CAI was able to reach the CC reservoir and affect the isotopic compositions of CC iron meteorites or that early outwardly migrating NC + CAI material could pass through this barrier (to pollute the CC reservoir) while later inwardly migrating CI material could not (as there appears to have been minimal CI material in the NC reservoir).

In the case where NC + CAI material made its way to the CC reservoir before CI material, the starting isotopic composition of the CC reservoir would have been NC-like (Ebert et al. 2018). Over time, this reservoir could have then been polluted by inwardly drifting CI material. As such, we would expect to have found larger P_{Cl} values at greater heliocentric distances at any given time (Figure 9(b)). Hence, the oldest CC iron meteorite parent bodies would have had to accrete at larger heliocentric distances than the younger CC iron meteorite parent bodies to explain the observed P_{Cl} values among these meteorites (Figure 9(c)). Once the barrier that created the NC–CC dichotomy was introduced and inwardly migrating material could start piling up against this feature, it is then possible for CC chondrites to all originate from a similar heliocentric distance as the isotopic composition of the innermost extent of the CC reservoir evolved (Figures 6 and 9(c)). As such, this model involves a change in the radial distance of CC planetesimal formation over time, from relatively distal and time-varying between ~ 1 and 1.5 Myr after CAI formation, to potentially relatively proximal and approximately constant at $\gtrsim 2$ Myr after CAI formation. As discussed in Section 3.3, the increase in P_{Cl} in CC chondrite parent bodies could also have been achieved by planetesimal accretion at increasing heliocentric distances.

The regimes in which gas and dust dynamically evolved throughout the disk, in which different generations of material were added to this structure, and in which planetesimals accreted in the CC reservoir are all currently uncertain, limiting our understanding of the origins in the evolution of the value of P_{Cl} over time. However, improved knowledge of both the introduction and motion of dust and gas throughout the protoplanetary disk as well as the formation distances of different planetesimals in the CC reservoir over time could help to distinguish between these two proposed models and uncover new constraints on the early evolution of our solar system.

4. Conclusions

1. Using a compilation of previously measured elemental and isotopic concentrations of CC meteorites (chondrites and iron meteorites) and the components of CC chondrites, we develop an inverse mixing model for the origin of the isotopic and elemental concentrations of these meteorites.
2. Whereas elemental and isotopic compositions of refractory elements in CC chondrites and the chondrite-like precursors to CC iron meteorites predominantly reflect the mixture of CAI material and preaccretionary bulk NC chondrite material (Gerber et al. 2017; Burkhardt et al. 2019), here we find that the elemental and isotopic compositions of the main component and plateau volatile elements in CC chondrites and the chondrite-like

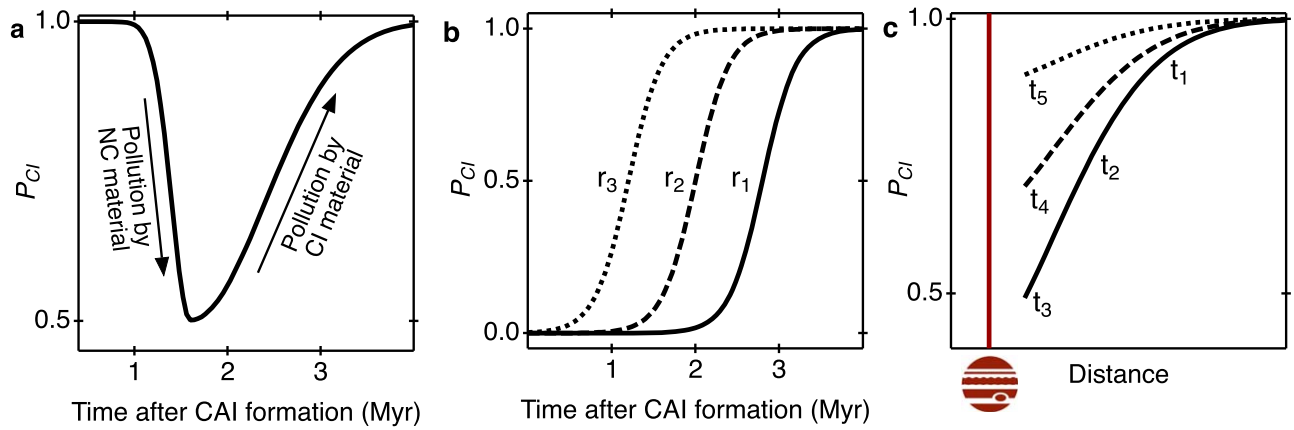


Figure 9. Model evolutions for the value of P_{CI} throughout the CC reservoir. (a) The evolution of P_{CI} at a given heliocentric distance for the case where the CC reservoir initially exhibited a CI isotopic composition that was subsequently polluted by outwardly drifting NC + CAI material, followed by inwardly drifting distal CI material. (b) The expected evolution of P_{CI} at three heliocentric distances (r_1 , r_2 , and r_3 , where $r_1 < r_2 < r_3$) for the case where the CC reservoir initially had an NC isotopic composition ($P_{CI} = 0$) and was polluted by inwardly drifting distal CI material. (c) The model in (b) shown as a function of radial distance, indicating the timing and location that CC parent bodies formed (t_1 is earliest, t_5 is latest). Initially, CC iron meteorites formed at similar enough times that their accretion locations very likely had to have varied, with the oldest of these bodies accreting at larger heliocentric distances (solid line, t_1 to t_3). As CI material drifted inwards and piled up against the NC-CC barrier (nominally indicated by Jupiter and the vertical red line) and the P_{CI} value could have increased over time (dashed line: intermediate times; dotted line: youngest times), CC chondrite parent bodies could then all originate from similar radial distance close to the NC-CC barrier (times t_4 and t_5).

precursors to CC iron meteorites originate from the mixture of bulk NC chondrite material with varying proportions of dust with an isotopic composition similar to CI chondrites. As such, the overall composition of primitive CC meteorites across most elements appears to originate from the mixture of NC, CI, and CAI material, in varying proportions.

3. The proportion of CI material in CC chondrites argues that chondrules in CO, CV, CM, and TL chondrites share near-identical Cr isotopic compositions. Given that the Cr isotopic composition of the disk is expected to have evolved over space and time (Sugiura & Fujiya 2014), this similarity argues that new CO, CV, CM, and TL chondrules did not form in the CC reservoir, and instead, that chondrules in these meteorites formed through the remelting of preexisting NC chondrules over a limited spatial extent and short time interval. Because CC chondrules contain lower proportions of CI material than the matrices of any measured CC chondrite and because CI material has been suggested to be associated with distal regions of the disk, the remelting of NC chondrules to form CC chondrules appears to have occurred relatively proximally in the CC reservoir. Together, all of these observations argue for a distinct and localized CC chondrule remelting event close to the barrier that introduced the NC-CC dichotomy. This disfavors chondrule generation mechanisms in the CC reservoir that are expected to have produced chondrules continuously over a range of radial distances (e.g., nebula lightning, bow shocks, planetary motion, etc.).
4. The CR chondrites are not simple mixtures of NC, CI, and CAI material, arguing that their constituents formed through mechanisms different from those in CO, CV, CM, and TL chondrites. The CR chondrites contain lower $\epsilon^{54}\text{Cr}$ values and plateau volatile element concentrations than predicted from their observed matrix abundances. This is consistent with the transformation of the matrix into chondrules in these meteorites, which may potentially have been caused by the melting of the matrix

during an energetic impact between two asteroid-sized bodies.

5. Together, the recovered proportions of CI material in CC iron meteorites and CC chondrites produce a time-resolved record of the amount of CI material throughout the CC reservoir. This record argues either for a change in the predominant direction of the flow and dust and gas within the first ~ 10 au of the disk over time (from outward between ~ 0 and 2 Myr after CAI formation, to inward at $\gtrsim 2$ Myr after CAI formation) or an evolution in the radial distances of asteroid accretion in the CC reservoir (from relatively distal and time-varying between ~ 1 –1.5 Myr after CAI formation, to approximately constant and relatively proximal at $0 \gtrsim 2$ Myr after CAI formation).

The authors thank Thorsten Kleine, Jan Render, and Oliver Shorttle for fruitful discussions. The authors also acknowledge the editor for efficient handling of the manuscript and an anonymous reviewer for their constructive comments. This study was performed under the auspices of the US Department of Energy by Lawrence Livermore National Laboratory under contract DE-AC52-07NA27344 with release number LLNL-JRNL-818033.

Appendix CC Meteorite Mixing Model

This appendix presents the mathematical details of a mixing model between bulk NC chondrite material (a preaccretionary mixture of NC chondrules and NC dust that is dominated by chondrules) and CI dust. This model can be used to determine whether the elemental concentrations, isotopic concentrations, and matrix mass fractions of CC meteorites are consistent with mixing between these components and so can be used to explore the origins of the $P_{CI, Cr}$, $P_{CI, Ni}$, $P_{CI, vtl}$, and χ values measured among these meteorites. The symbols and definitions adopted for each parameter in this model and throughout this study are presented in Table 4.

Table 4
Summary of Parameters Used in the Mixing Model and throughout This Study

Symbol	Definition	Equation Used to Recover the Parameter
P_{CI}	General term used to describe the mass fraction of CI material in a bulk CC chondrite. It can refer to either $P_{CI,Cr}$ or $P_{CI,Ni}$.	
$P_{CI,Cr}$	Mass fraction of CI material in a bulk CC chondrite recovered from its Cr isotopic concentration	Equations (1) and (2)
$P_{CI,Ni}$	Mass fraction of CI material in a bulk CC chondrite recovered from its Ni isotopic concentration	Equations (1) and (2)
$P_{CI,vil}$	Mass fraction of CI material in a bulk CC chondrite recovered from its plateau volatile element concentrations	Equation (1)
P_{CAI}	Mass fraction of CAI material recovered from either the bulk Ti isotopic and elemental compositions of CC chondrites or the bulk Mo isotopic and elemental compositions of CC iron meteorites	Equations (1) and (2)
$P_{CI,m}$	Average mass fraction of CI material in the matrix of a CC chondrite recovered from its bulk isotopic and elemental Cr concentrations	Equation (9)
ΔP_{CI}	$P_{CI,Cr} - P_{CI,vil}$	
α	Mass fraction of CI dust incorporated into CC chondrite matrix	
β	Average mass fraction proportion of CI material in chondrules in a given CC chondrite calculated using their average elemental and isotopic Cr concentrations	
γ	Mass fraction of matrix in an NC chondrite	
χ	Mass fraction of matrix in a CC chondrite	
φ	$\frac{I_{NC,c}C_{NC,c} - I_{CI}C_{CI}}{I_{NC,b}C_{NC,b} - I_{CI}C_{CI}}$	
$I_{NC,b}$ ^{a,b}	Bulk isotopic concentration of an NC chondrite	
$I_{NC,m}$ ^{a,b}	Average isotopic concentration of the matrix in an NC chondrite	
$I_{NC,c}$ ^{a,b}	Average isotopic concentration of chondrules in an NC chondrite	
$C_{NC,b}$ ^{a,b}	Bulk elemental concentration of an NC chondrite	
$C_{NC,m}$ ^{a,b}	Average elemental concentration of the matrix in an NC chondrite	
$C_{NC,c}$ ^{a,b}	Average elemental concentration of chondrules in an NC chondrite	
$I_{CC,b}$ ^{a,b}	Bulk isotopic concentration of a CC chondrite	
$I_{CC,m}$ ^{a,b}	Average isotopic concentration of the matrix in a CC chondrite	
$I_{CC,c}$ ^{a,b}	Average isotopic concentration of chondrules in a CC chondrite	
$C_{CC,b}$ ^{a,b}	Bulk elemental concentration of a CC chondrite	
$C_{CC,m}$ ^{a,b}	Average elemental concentration of the matrix in a CC chondrite	
$C_{CC,c}$ ^{a,b}	Average elemental concentration of chondrules in a CC chondrite	
I_{CI} ^{a,b}	Bulk isotopic concentration of CI chondrites	
C_{CI} ^{a,b}	Bulk elemental concentration of CI chondrites	

Notes.

^a Value presented in Table 1.

^b Inclusion of ' indicates the concentration of plateau volatile elements.

Considering that the two main components that govern the isotopic signature of main component elements in a chondrite are chondrules and matrix, the main component element isotopic composition of a bulk NC chondrite, $I_{NC,b}$, can be expressed as

$$I_{NC,b}C_{NC,b} = I_{NC,m}C_{NC,m}\gamma + I_{NC,c}C_{NC,c}(1 - \gamma), \quad (A1)$$

where γ is the mass fraction of matrix in NC chondrites (5 wt%, Table 5), $I_{NC,m}$ and $I_{NC,c}$ are the main component element isotopic compositions of NC matrix and NC chondrules, respectively, and $C_{NC,b}$, $C_{NC,m}$, and $C_{NC,c}$ are the main component elemental concentrations of bulk NC chondrites, NC matrix, and NC chondrules, respectively. Similarly, for CC chondrites,

$$I_{CC,b}C_{CC,b} = I_{CC,m}C_{CC,m}\chi + I_{CC,c}C_{CC,c}(1 - \chi), \quad (A2)$$

where χ is the mass fraction of matrix in a CC chondrite, $I_{CC,b}$, $I_{CC,m}$, and $I_{CC,c}$ are the main component element isotopic concentrations of a bulk CC chondrite, CC matrix, and CC chondrules in a given group, respectively, and $C_{CC,b}$, $C_{CC,m}$, and $C_{CC,c}$ are the main component elemental concentrations in bulk CC chondrites, CC matrix, and CC chondrules in a given CC chondrite group, respectively. In the case where bulk CC

Table 5
Values of Matrix Volume Fraction, Bulk Density, Grain Density, Calculated Matrix Mass Proportion, and Nominal Uncertainty on Matrix Mass Fraction for CC and OC Chondrites

	V (vol%)	ρ_b (kg m ⁻³)	ρ_g (kg m ⁻³)	χ, γ (wt%)	Uncertainty on χ (wt%)
CI	100 ^a	1550 ^d	2450 ^d	100	0
CM	70 ^a	2300 ^d	2900 ^d	62	12.6
CO	32.5 ^a	3000 ^d	3500 ^d	21	11.7
CV	40 ^a	3000 ^d	3500 ^d	30	11.7
CR	35 ^b	3100 ^d	3400 ^d	29	11
TL	83 ^c	1800 ^c	2550 ^c	76	14.1
OC	12.5 ^a	3350 ^d	3650 ^d	5	10.9

Notes.

^a Scott & Krot (2014).

^b Schrader et al. (2011).

^c Ralchenko et al. (2014).

^d Macke et al. (2011).

chondrites are a mixture of bulk NC chondrite material and CI dust, and where some CI material is incorporated into CC chondrules when they experienced remelting, the isotopic

composition of a bulk CC chondrite can be expressed as

$$I_{CC,b}C_{CC,b} = I_{CI}C_{CI}\alpha + I_{NC,m}C_{NC,m}\gamma(1 - \alpha) + (1 - \gamma)(1 - \alpha)(I_{CI}C_{CI}\beta + I_{NC,m}C_{NC,m}(1 - \beta)), \quad (A3)$$

where α is the mass fraction of CI dust incorporated into CC chondrite matrix, and I_{CI} and C_{CI} are the main component element isotopic composition and elemental concentration in CI chondrites, respectively. β is the mass fraction of CI material incorporated into CC chondrules, which can be calculated as

$$\beta = \frac{I_{CC,c}C_{CC,c} - I_{NC,b}C_{NC,b}}{I_{CI}C_{CI} - I_{NC,b}C_{NC,b}}, \quad (A4)$$

and in the case of Cr is equal to 0.57 for $I_{CC,c} = 0.58$ (the average of CV pooled chondrules) and $C_{CC,c} = 2960$ ppm (Schneider et al. 2020). The value of $P_{CI,Cr}$ is then calculated as

$$P_{CI,Cr} = \frac{I_{CC,b}C_{CC,b} - I_{NC,b}C_{NC,b}}{I_{CI}C_{CI} - I_{NC,b}C_{NC,b}}, \quad (A5)$$

which can be expressed as

$$P_{CI,Cr} = \alpha + \varphi(1 - \gamma)(1 - \alpha)\beta, \quad (A6)$$

where

$$\varphi = \frac{I_{NC,c}C_{NC,c} - I_{CI}C_{CI}}{I_{NC,b}C_{NC,b} - I_{CI}C_{CI}}. \quad (A7)$$

Using the values of $I_{NC,c}$ and $C_{NC,c}$ reported by Schneider et al. (2020), the calculated value of $\varphi \approx 1$. Additionally, by comparing Equations (A2) and (A3),

$$\alpha = \frac{\chi - \gamma}{1 - \gamma} \quad (A8)$$

such that

$$P_{CI,Cr} = \frac{\chi - \gamma}{1 - \gamma} + \varphi(1 - \chi)\beta. \quad (A9)$$

For the case of plateau volatile elements, including OC chondrites in the analysis performed by Hellmann et al. (2020) demonstrates that chondrules in both OC and CC chondrites (excluding CR chondrites) contain concentrations of plateau volatile elements that are ~ 13 wt% that of CI chondrites. As such, there appears to have been minimal to no incorporation of these elements into NC chondrules when they were remelted and exchanged material with the local dust and gas in the disk to form CC chondrules in this model. Hence, the volatile element concentration of a bulk CC chondrite, $C'_{CC,b}$, that is a mixture of bulk NC chondrite material and CI dust can be expressed as

$$C'_{CC,b} = C'_{CI}\alpha + C'_{NC,m}\gamma(1 - \alpha) + C'_{NC,c}(1 - \gamma)(1 - \alpha), \quad (A10)$$

where $C'_{CC,b}$, C'_{CI} , $C'_{NC,m}$, and $C'_{NC,c}$ are the plateau volatile elemental concentrations in a bulk CC chondrite, CI chondrites, NC matrix, and NC chondrules, respectively. The value of $P_{CI,vil}$ can be calculated as

$$P_{CI,vil} = \frac{C'_{CC,b} - C'_{NC,b}}{C'_{CI} - C'_{NC,b}}, \quad (A11)$$

which can be expressed as

$$P_{CI,vil} = \alpha = \frac{\chi - \gamma}{1 - \gamma}. \quad (A12)$$

As such,

$$P_{CI,Cr} = P_{CI,vil} + \varphi(1 - \chi)\beta \quad (A13)$$

and the difference in the proportions of CI material recovered from the Cr isotopic compositions and the plateau volatile element concentrations, $\Delta P_{CI} = P_{CI,Cr} - P_{CI,vil}$, can be expressed as

$$\Delta P_{CI} = \varphi(1 - \chi)\beta \approx (1 - \chi)\beta. \quad (A14)$$

Hence, for the case where the bulk composition of a CC chondrite originates from mixing bulk NC chondrite material and CI dust, the difference in the proportions of CI material recovered from Cr isotopic composition and plateau volatile element concentrations is due to the mass fraction of chondrules $(1 - \chi)$ that is present in a chondrite and the mass fraction of CI material incorporated into these chondrules.

The mass fraction of matrix in a chondrite can be calculated from its volume fraction, which has been recovered from petrographic observations for a large number of chondrites, using

$$\chi = V \frac{\rho_m}{\rho_b}, \quad (A15)$$

where ρ_m is the density of the matrix, ρ_b is the bulk density of a chondrite, and V is the matrix volume fraction (Hellmann et al. 2020). The density of the matrix can be calculated from

$$\rho_b = \rho_m V + \rho_{nm}(1 - V), \quad (A16)$$

where ρ_{nm} is the density of the nonmatrix component, which is assumed to be equal to the grain density of a given chondrite, ρ_g . This leads to the relationship

$$\chi = 1 - \frac{\rho_g}{\rho_b}(1 - V). \quad (A17)$$



The same relationship is also true for γ in NC chondrites. Our adopted values of V , ρ_g , and ρ_b , and our calculated values of χ and γ are presented in Table 5. The values of V for CI, CM, CO, CV, CR, and OC chondrites are all taken from petrographic observations. The value of V for the TL chondrite recovered from petrographic observations varies widely among the different stones of this meteorite (50–90 vol%) and even among different thin sections of the same stone (Blinova et al. 2014b). As such, it is unclear whether the average value of V calculated from these limited petrographic observations of a few thin sections is representative of the whole meteorite. Hence, we chose to calculate the average V value for this meteorite using

$$\phi_b = \phi_m V + \phi_{nm}(1 - V), \quad (A18)$$

where ϕ_b , ϕ_m , and ϕ_{nm} are the porosities of the bulk sample, matrix, and nonmatrix components, respectively. The porosities of 11 whole stones of Tagish Lake with masses ranging from 8 to 60 g have previously been measured, so this approach is expected to yield a far more representative value of V for this meteorite than limited petrographic observations. We used a value of $\phi_b = 0.29$ (the average value recovered from 11 stones

of Tagish Lake; Ralchenko et al. 2014) and assumed a value of $\phi_{nm}=0$ (supported by the low observed porosities of chondrules; Lewis et al. 2018) and $\phi_m=0.35$ (matching the value measured from CI chondrites, which are also high-porosity, saponite-bearing chondrites; Macke et al. 2011). This approach yields a value of $V=83$ vol% for TL, which is at the higher end of the range of values identified from petrographic observations of this meteorite.

ORCID iDs

James F. J. Bryson  <https://orcid.org/0000-0002-5675-8545>
 Gregory A. Brennecka  <https://orcid.org/0000-0002-0852-5595>

References

- Alexander, C. M. O. 2019a, *GeCoA*, 254, 277
 Alexander, C. M. O. 2019b, *GeCoA*, 254, 246
 Alexander, C. M. O., Greenwood, R. C., Bowden, R., et al. 2018a, *GeCoA*, 221, 406
 Alexander, C. M. O., Howard, K. T., Bowden, R., & Fogel, M. L. 2013, *GeCoA*, 123, 244
 Alexander, C. M. O., McKeegan, K. D., & Altwegg, K. 2018b, *SSRv*, 214, 36
 Barrat, J. A., Zanda, B., Moynier, F., et al. 2012, *GeCoA*, 83, 79
 Bermingham, K. R., Furi, E., Lodders, K., & Marty, B. 2020, *SSRv*, 216, 133
 Bermingham, K. R., Worsham, E. A., & Walker, R. J. 2018, *E&PSL*, 487, 221
 Bischoff, A., Palme, H., Ash, R., et al. 1993, *GeCoA*, 57, 1587
 Bischoff, A., Vogel, N., & Roszjar, J. 2011, *ChEG*, 71, 101
 Bland, P. A., Alard, O., Benedix, G. T., et al. 2005, *PNAS*, 102, 13755
 Blinova, A. I., Herd, C. D. K., & Duke, M. J. M. 2014a, *M&PS*, 49, 1100
 Blinova, A. I., Zega, T. J., Herd, C. D. K., & Stroud, R. M. 2014b, *M&PS*, 49, 473
 Bollard, J., Connelly, J. N., Whitehouse, M. J., et al. 2017, *SciA*, 3, e1700407
 Bollard, J., Kawasaki, N., Sakamoto, N., et al. 2019, *GeCoA*, 260, 62
 Brasser, R., & Mojzsis, S. J. 2020, *NatAs*, 4, 492
 Braukmuller, N., Wombacher, F., Funk, C., & Munker, C. 2019, *NatGe*, 12, 564
 Braukmuller, N., Wombacher, F., Hezel, D. C., Escoube, R., & Munker, C. 2018, *GeCoA*, 239, 17
 Brennecka, G. A., Burkhardt, C., Budde, G., et al. 2020, *Sci*, 370, 837
 Brown, P. G., Hildebrand, A. R., Zolensky, M. E., et al. 2000, *Sci*, 290, 320
 Brownlee, D., Tsou, P., Al  on, J., et al. 2006, *Sci*, 314, 1711
 Bryson, J. F. J., Neufeld, J. A., & Nimmo, F. 2019, *E&PSL*, 521, 68
 Bryson, J. F. J., Weiss, B. P., Biersteker, J. B., King, A. J., & Russell, S. S. 2020a, *ApJ*, 896, 103
 Bryson, J. F. J., Weiss, B. P., Lima, E. A., Gattacceca, J., & Cassata, W. 2020b, *ApJ*, 892, 126
 Budde, G., Burkhardt, C., Brennecka, G. A., et al. 2016, *E&PSL*, 454, 293
 Budde, G., Burkhardt, C., & Kleine, T. 2019, *NatAs*, 3, 736
 Budde, G., Kruijer, T. S., & Kleine, T. 2018, *GeCoA*, 222, 284
 Burkhardt, C., Dauphas, N., Hans, U., Bourdon, B., & Kleine, T. 2019, *GeCoA*, 261, 145
 Burkhardt, C., Kleine, T., Oberli, F., et al. 2011, *E&PSL*, 312, 390
 Choe, W. H., Huber, H., Rubin, A. E., Kallemeyn, G. W., & Wasson, J. T. 2010, *M&PS*, 45, 531
 Ciesla, F. 2007, *Sci*, 318, 613
 Ciesla, F. J. 2009, *Icar*, 200, 655
 Clayton, R. N., & Mayeda, T. K. 1999, *GeCoA*, 63, 2089
 Connelly, J. N., Bizzarro, M., Krot, A. N., et al. 2012, *Sci*, 338, 651
 Connelly, J. N., Bollard, J., & Bizzarro, M. 2017, *GeCoA*, 201, 345
 Creech, J. B., & Moynier, F. 2019, *ChGeo*, 511, 81
 Dauphas, N., Remusat, L., Chen, J. H., et al. 2010, *ApJ*, 720, 1577
 Davidson, J., Alexander, C. M. O., Stroud, R. M., Busemann, H., & Nittler, L. R. 2019a, *GeCoA*, 265, 259
 Davidson, J., Schrader, D. L., Alexander, C. M. O., Nittler, L. R., & Bowden, R. 2019b, *GeCoA*, 267, 240
 Davis, A. M., Zhang, J., Greber, N. D., et al. 2018, *GeCoA*, 221, 275
 Desch, S. J., Kalyaan, A., & Alexander, C. M. O. 2018, *ApJS*, 238, 11
 Dobrica, E., & Brearley, A. J. 2020, *M&PS*, 55, 649
 Doyle, P. M., Jogo, K., Nagashima, K., et al. 2015, *NatCo*, 6, 7444
 Ebert, S., Render, J., Brennecka, G. A., et al. 2018, *E&PSL*, 498, 257
 Fehr, M. A., Hammond, S. J., & Parkinson, I. J. 2018, *GeCoA*, 222, 17
 Fischer-Godde, M., & Kleine, T. 2017, *Natur*, 541, 525
 Frank, D., Zolensky, M., Martinez, J., et al. 2011, *LPSC*, 42, 2785
 Friedrich, J. M., Wang, M. S., & Lipschutz, M. E. 2002, *M&PS*, 37, 677
 Fujiya, W., Hoppe, P., Ushikubo, T., et al. 2019, *NatAs*, 3, 910
 Gattacceca, J., Bonal, L., Sonzogni, C., & Longerey, J. 2020, *E&PSL*, 547, 116467
 Gerber, S., Burkhardt, C., Budde, G., Metzler, N., & Kleine, T. 2017, *ApJL*, 841, L17
 G  pel, C., Birck, J. L., Galy, A., Barrat, J. A., & Zanda, B. 2015, *GeCoA*, 156, 1
 Gounelle, M., Morbidelli, A., Bland, P. A., et al. 2008, in *The Solar System beyond Neptune*, ed. M. A. Barucci, H. Boehnhardt, & D. P. Cruikshank (Tucson, AZ: Univ. Arizona Press), 525
 Gounelle, M., & Zolensky, M. E. 2014, *M&PS*, 49, 1769
 Gregory, T., Luu, T.-H., Coath, C. D., Russell, S. S., & Elliott, T. 2020, *SciA*, 6, eaay9626
 Hartmann, L., Calvert, N., Gullbring, E., & D'Alessio, P. 1998, *ApJ*, 495, 385
 Hellmann, J. L., Hopp, T., Burkhardt, C., & Kleine, T. 2020, *E&PSL*, 549, 116508
 Herd, C. D. K., Sharp, Z. D., Alexander, C. M. O., & Blinova, A. 2012, *LPSC*, 43, 1688
 Hevey, P. J., & Sanders, I. S. 2006, *M&PS*, 41, 95
 Hewins, R. H., Bourrot-Denise, M., Zanda, B., et al. 2014, *GeCoA*, 124, 190
 Howard, K. T., Alexander, C. M. O., Scharder, D. L., & Dyl, K. A. 2015, *GeCoA*, 149, 206
 Jacquet, E., Barrat, J. A., Beck, P., et al. 2016, *M&PS*, 51, 851
 Jarosewich, E. 1990, *Metic*, 25, 323
 Jarosewich, E., Clarke, R. S., & Barrows, J. N. 1987, *SmCES*, 27, 1
 Johnson, B. C., Minton, D. A., Melosh, H. J., & Zuber, M. T. 2015, *Natur*, 517, 339
 Joswiak, D. J., Brownlee, D. E., Nguyen, A. N., & Messenger, S. 2017, *M&PS*, 52, 1612
 Kadlag, Y., Becker, H., & Harbott, A. 2019, *M&PS*, 54, 2116
 Kallemeyn, G. W., Rubin, A. E., & Wasson, J. T. 1991, *GeCoA*, 55, 881
 Kallemeyn, G. W., Rubin, A. E., & Wasson, J. T. 1994, *GeCoA*, 58, 2873
 Kallemeyn, G. W., Rubin, A. E., & Wasson, J. T. 1996, *GeCoA*, 60, 2243
 King, A. J., Schofield, P. F., Howard, K. T., & Russell, S. S. 2015, *GeCoA*, 165, 148
 King, A. J., Schofield, P. F., & Russell, S. S. 2017, *M&PS*, 52, 1197
 Kita, N. T., Nagahara, H., Tachibana, S., et al. 2010, *GeCoA*, 74, 6610
 Kleine, T., Budde, G., Burkhardt, C., et al. 2020, *SSRv*, 216, 55
 Kong, P., Mori, T., & Ebihara, M. 1997, *GeCoA*, 61, 4895
 Krot, A. N., Amelin, Y., Cassen, P., & Meibom, A. 2005, *Natur*, 436, 989
 Krot, A. N., Meibom, A., Wiesberg, M. K., & Keil, K. 2002, *M&PS*, 37, 1451
 Kruahashi, E., Kita, N. T., Nagahara, H., & Morishita, Y. 2008, *GeCoA*, 72, 3865
 Kruijer, T. S., Burkhardt, C., Budde, G., & Kleine, T. 2017, *PNAS*, 114, 6712
 Kruijer, T. S., Kleine, T., & Borg, L. E. 2019, *NatAs*, 4, 32
 Lambrechts, M., & Johansen, A. 2014, *A&A*, 572, A107
 Laul, J., Case, D., Schmidt-Bleek, F., & Lipschutz, M. 1970, *GeCoA*, 34, 89
 Lewis, J. A., Jones, R. H., & Garcea, S. C. 2018, *GeCoA*, 240, 293
 Lichtenberg, T. O., Drazkowska, J., Sch  nb  chler, M., Golabek, G. J., & Hands, T. O. 2021, *Sci*, 371, 365
 Lodders, K. 2003, *ApJ*, 591, 1220
 Lodders, K., & Fegley, B. 1998, *The Planetary Scientist's Companion* (Oxford: Oxford Univ. Press)
 Luck, J. M., Othman, D. B., & Albarede, F. 2005, *GeCoA*, 69, 5351
 Macke, R. J., Consolmagno, G. J., & Britt, D. T. 2011, *M&PS*, 46, 1842
 Mason, B., & Wiik, H. B. 1962, *Am. Mus. Novit.*, 2106, 1, <http://digitallibrary.amnh.org/handle/2246/3409>
 Morbidelli, A. 2020, *A&A*, 638, A1
 Nagashima, K., Krot, A. N., & Huss, G. R. 2014, *GeocJ*, 48, 561
 Nanne, J. A. M., Nimmo, F., Cuzzi, J. N., & Kleine, T. 2019, *E&PSL*, 511, 44
 Noguchi, T. 1993, *AMR*, 6, 204
 Olsen, M. B., Wielandt, D., Schiller, M., Van Kooten, E. M. M. E., & Bizzarro, M. 2016, *GeCoA*, 191, 118
 Palme, H., Lodders, K., & Jones, A. 2014, in *Planets, Asteroids, Comets and The Solar System, Treatise on Geochemistry*, Vol. 2, ed. A. M. Davis (Amsterdam: Elsevier), 15
 Pape, J., Mezger, K., Bouvier, A. S., & Baumgartner, L. P. 2019, *GeCoA*, 244, 416
 Petit, M., Birck, J. L., Luu, T. H., & Gounelle, M. 2011, *ApJ*, 736, 23
 Piani, L., Marrocchi, Y., Rigaudier, T., et al. 2020, *Sci*, 369, 1110
 Pringle, E. A., & Moynier, F. 2017, *E&PSL*, 473, 62
 Pringle, E. A., Moynier, F., Beck, P., Paniello, R., & Hezel, D. C. 2017, *E&PSL*, 468, 62

- Qin, L., Alexander, C. M. O., Carlson, R. W., Horan, M. F., & Yokoyama, T. 2010, *GeCoA*, **74**, 1122
- Ralchenko, M., Britt, D. T., Samson, C., et al. 2014, *LPSC*, **45**, 1021
- Render, J., Brennecka, G. A., Wang, S.-J., Wasylenko, L. E., & Kleine, T. 2018, *ApJ*, **826**, 26
- Rubin, A. E., Trigo-Rodriguez, J. M., Huber, H., & Wasson, J. T. 2007, *GeCoA*, **71**, 2361
- Rubin, A. E., & Wasson, J. T. 1987, *GeCoA*, **51**, 1923
- Russell, S. D. J., Longstaffe, F. J., King, P. L., & Larson, T. E. 2010, *GeCoA*, **74**, 2484
- Schiller, M., Bizzarro, M., & Assis Fernandes, V. 2018, *Natur*, **555**, 507
- Schneider, J. M., Burkhardt, C., Marrocchi, Y., Brennecka, G. A., & Kleine, T. 2020, *E&PSL*, **551**, 116585
- Schönbächler, M., Carlson, R. W., Horan, M. F., Mock, T. D., & Hauri, E. H. 2008, *GeCoA*, **72**, 5330
- Schrader, D. L., Davidson, J., Greenwood, R. C., Franchi, I. A., & Gibson, J. M. 2014, *E&PSL*, **407**, 48
- Schrader, D. L., Franchi, I. A., Connolly, H. C., et al. 2011, *GeCoA*, **75**, 308
- Schrader, D. L., Nagashima, K., Davidson, J., et al. 2020, *GeCoA*, **282**, 133
- Schrader, D. L., Nagashima, K., Krot, A. N., et al. 2017, *GeCoA*, **201**, 275
- Scott, E. R. D., & Krot, A. N. 2014, in *Meteorites, Comets, and Planets, Treatise on Geochemistry*, Vol. 1, ed. H. D. Holland & K. K. Turekian (Amsterdam: Elsevier), 143
- Scott, E. R. D., Krot, A. N., & Sanders, I. S. 2018, *ApJ*, **854**, 164
- Shukolyukov, A., & Lugmair, G. W. 2006, *E&PSL*, **250**, 200
- Spitzer, F., Burkhardt, C., Budde, G., et al. 2020, *ApJL*, **898**, L2
- Steele, R. C. J., Coath, C. D., Regelous, M., Russell, S. S., & Elliott, T. 2012, *ApJ*, **758**, 59
- Stracke, A., Palme, H., Gellissen, M., et al. 2012, *GeCoA*, **85**, 114
- Sugiura, N., & Fujiya, W. 2014, *M&PS*, **49**, 772
- Tang, H., & Dauphas, N. 2014, *E&PSL*, **390**, 264
- Trinquier, A., Birck, J. L., & Allègre, C. J. 2007, *ApJ*, **655**, 1179
- Trinquier, A., Elliott, T., Ulfbeck, D., et al. 2009, *Sci*, **324**, 374
- Ushikubo, T., & Kimura, M. 2021, *GeCoA*, **293**, 328
- Van Kooten, E. M. M. E., & Moynier, F. 2019, *GeCoA*, **261**, 248
- Van Kooten, E. M. M. E., Moynier, F., & Agranier, A. 2019, *PNAS*, **116**, 18860
- Van Kooten, E. M. M. E., Wielandt, D., Schiller, M., et al. 2016, *PNAS*, **113**, 2011
- Wang, H., Weiss, B. P., Bai, X.-N., et al. 2017, *Sci*, **355**, 623
- Wang, Z., Becker, H., & Wombacher, F. 2015, *Geostand. Geoanal. Res.*, **39**, 185
- Warren, P. H. 2011, *E&PSL*, **311**, 93
- Wasson, J. T., Isa, J., & Rubin, A. E. 2013, *GeCoA*, **108**, 45
- Wasson, J. T., & Kallemeyn, G. W. 1988, *RSPTA*, **A325**, 535
- Wiesberg, M. K., & Huber, H. 2007, *M&PS*, **42**, 1495
- Williams, C. D., Sanborn, M. E., Defouilloy, C., et al. 2020, *PNAS*, **117**, 23426
- Wolf, D., & Palme, H. 2001, *M&PS*, **36**, 559
- Wolf, S. F., Unger, D. L., & Friedrich, J. M. 2005, *Anal. Chim. Acta*, **528**, 121
- Wood, B. J., Smythe, D. J., & Harrison, T. 2019, *AmMin*, **104**, 844
- Wood, J. A. 2004, *GeCoA*, **68**, 4007
- Worsham, E. A., Burkhardt, C., Budde, G., et al. 2019, *E&PSL*, **521**, 103
- Yamanobe, M., Nakamura, T., & Nakasima, D. 2018, *PolSc*, **15**, 29
- Zhang, J., Dauphas, N., Davis, A. M., Leya, I., & Fedkin, A. 2012, *NatGe*, **5**, 251
- Zhang, J., Dauphas, N., Davis, A. M., & Pourmand, A. 2011, *J. Anal. At. Spectrosc.*, **26**, 2197
- Zhu, K., Liu, J., Moynier, F., et al. 2019, *ApJ*, **873**, 82